ACTIVE NOISE CONTROL USING MODALLY TUNED PHASE-COMPENSATED FILTERS

by

Jesse B. Bisnette

BS, University of Pittsburgh, 2002

Submitted to the Graduate Faculty of

the School of Engineering in partial fulfillment

of the requirements for the degree of

Master of Science

University of Pittsburgh

2003

UNIVERSITY OF PITTSBURGH

SCHOOL OF ENGINEERING

This thesis was presented

by

Jesse B. Bisnette

It was defended on

25 November 2003

and approved by

Jeffery S. Vipperman, Assistant Professor, Mechanical Engineering

Danial D. Budny, Associate Professor, Civil Engineering

William W. Clark, Associate Professor, Mechanical Engineering

Thesis Advisor: Jeffery S. Vipperman, Assistant Professor, Mechanical Engineering

ACTIVE NOISE CONTROL USING MODALLY TUNED PHASE-COMPENSATED FILTERS

Jesse B. Bisnette, MS

University of Pittsburgh, 2003

An active noise control device or an active noise absorber (ANA) that is based on either resonant 2^{nd}-order or 4^{th}-order Butterworth filters is developed and demonstrated. This control method is similar to structural positive position feedback (PPF) control, with two exceptions: 1) acoustic transducers (microphone and speaker) cannot be truly colocated, and 2) the acoustic actuator (loudspeaker) has significant dynamics that can affect performance and stability. Acoustic modal control approaches are typically not sought, however, there are a number of applications where controlling a few room modes is adequate. A model of a duct with speakers at each end is developed and used to demonstrate the control method, including the impact of the speaker dynamics. An all-pass filter is used to provide phase compensation and to improve controller performance. Two companion experimental studies validated the simulation results. A single mode case using a resonant band-pass filter demonstrated nearly $10\,dB$ of control in the first duct, while a multimodal case using two 4^{th}-order Butterworth band-pass filters show both $10\,dB$ of reduction in the fundamental mode and nearly $8.0\,dB$ in the second.

TABLE OF CONTENTS

1.0 INTRODUCTION 1

2.0 MODELING THE SYSTEM 7

2.1 Analytical Model 7

2.1.1 Acoustic Duct 8

2.1.2 Loudspeakers 10

2.2 State Space Representation and Model Verification 11

2.2.1 Acoustic Duct State Matrices 13

2.2.2 Loudspeaker State Matrices 16

2.3 Simulated Plant Response and Model Verification 17

3.0 COMPENSATOR DESIGN 19

3.1 Feedback Configuration 19

3.2 Resonant Filter Design 21

3.2.1 Phase Compensation 24

3.2.2 Resonant Filter Control Simulation 25

3.3 Fourth-order Compensators 29

3.4 Control with Non-collocated Sensor/Actuator Pair 32

3.5 Multimodal Control 35

4.0 EXPERIMENTAL DEMONSTRATIONS 40

4.1 Design and Response of Second-order Controller 40

4.1.1 Compensator Design 40

4.1.2 Closed-loop Response 42

4.2 Design and Response of Multimodal Controller 43

5.0 CONCLUDING REMARKS 49
APPENDIX A. MATLAB™ CODE FOR DUCT 51
APPENDIX B. MATLAB™ CODE FOR LOUDSPEAKERS 54
APPENDIX C. MATLAB™ CODE UTILIZING DESIGN PROCEDURE 56
BIBLIOGRAPHY 62

LIST OF TABLES

1 Plant parameters used in simulation. 18
2 Dual mode controller design parameters. 38
3 Compensator parameters. 42
4 Multimodal Butterworth filter compensator parameters. 46

LIST OF FIGURES

1 Block diagram of PPF controller. 4
2 Response of a single mode structure and PPF filter. 5
3 Disturbance/Controlled response for a single mode structure. 5
4 Rigid walled acoustic duct setup. 7
5 Loudspeaker schematic. 10
6 Plant schematic showing system conventions. 12
7 Simulated and experimental results for disturbance-path. 18
8 Closed-loop system schematic. 20
9 Fully coupled feedback model of controller. 20
10 Simplified feedback model of controller. 21
11 Frequency response of control speaker, duct, and duct+loudspeaker. 22
12 Frequency response of control-path and low/band-pass filter. 23
13 Predicted disturbance-path/closed-loop response without speaker dynamics. . 26
14 Predicted disturbance-path/closed-loop response with speaker dynamics. . . . 27
15 Root locus analysis of first mode controller 28
16 Predicted disturbance-path/closed-loop response using all-pass filter. 28
17 Root locus analysis of second mode controller 29
18 Predicted disturbance-path/closed-loop response for control over mode 2. . . 30
19 Butterworth response tuned to second duct mode. 31
20 Predicted control-path response. 33
21 Root-locus of control-path with Butterworth filter. 33
22 Predicted closed-loop response with control over mode 2. 34

23 Illustration of sensor placement using duct mode shapes 35
24 Predicted results of duct+loudspeaker when $x_{sen} = x_1$. 36
25 Predicted disturbance-path/closed-loop results when $x_{sen} = x_1$, $x_e = x_2$. . . . 36
26 Schematic of multimodal controller. 37
27 Predicted control-path response tuned to modes 1 and 2. 39
28 Predicted disturbance-path/closed-loop response for control over modes 1 and 2. 39
29 Experimental test bed. 41
30 Schematic for inverting all-pass filter network. 42
31 Measured fully compensated control-path. 43
32 Measured disturbance-path/closed-loop response for various gain values. . . . 44
33 Measured Disturbance-path/closed-loop response over $500\,Hz$ frequency range. 45
34 Measured fully compensated multimodal control-path. 46
35 Measured disturbance-path/closed-loop response for various gain combinations. 48
36 Measured disturbance-path/closed-loop response for gain value $G3$. 48

NOMENCLATURE

Symbols

l : Length

w : Width

h : Height

V : Volume of duct

A : Area of speaker cone

x : Position

R : Resistance

L : Inductance

C : Capacitance

I : Current

m : Mass of loudspeaker cone

b : Damping ratio of loudspeaker

k : Stiffness of loudspeaker

Bl : Electro-mechanical coupling coefficient

c : Sound speed in air

N : Number of modes

t : Time

f : Frequency

$v(t)$: Applied voltage

$y(t)$: Speaker displacement function

$p(x,t)$: Pressure function

$\mathbf{A}$: State-space A matrix

$\mathbf{B}$: State-space B matrix

$\mathbf{C}$: State-space C matrix

$\mathbf{D}$: State-space D matrix

U : State input vector

F : Force

H : Transfer function

S : Laplace variable

G : Filter gain

z : Filter zero

p : Filter pole

μ : State variable

φ : State output vector

ρ_o : Density of air at room temperature

Ψ : Eigenfunction of duct

ϕ : Structural/acoustical coupling coefficient

β : State duct model input coefficients

γ : State duct model pressure output coefficents

ω : Circular frequency

ζ : Damping ratio

θ : Phase angle

Subscripts

n : Mode index, or referring to noise speaker

j : Speaker index

co : Cuttoff frequency

d : Referring to duct

e : Referring to error signal

s : Referring to loudspeaker

sen : Referring to sensor signal

c : Referring to compensator, or control speaker

f : Referring to generic filter

a : Referring to all-pass filter

g : Referring to gain circuit

LP : Low-pass filter

BP : Band-pass filter

AP : All-pass filter

Superscripts

$\dot{}$: First derivative, $\frac{d}{dt}$

$\ddot{}$: Second Derivative, $\frac{d^2}{dt^2}$

1.0 INTRODUCTION

Engineering noise control typically entails reducing sound by modifying acoustic sources, augmenting transmission paths, or removing the object or subject being exposed to noise. Within a reverberant enclosure, both passive and active control technologies can be applied either separately or in combination [1].

Passive control techniques are an attractive solution when a power source is either unwanted or impractical. Often, passive control is achieved by adding absorptive materials such as foam insulation or ceiling tiles to the system so that the material disrupts the reflection of the disturbance sound field. Another popular method used in passive control is the Helmholtz resonator, in which a mechanical band-stop filter is achieved by adding a small opening in a cavity such as a duct or pipe which leads to a fixed volume chamber tuned to a given frequency [2, 3]. Some implementations of Helmholtz resonators include the ability to actively tailor the passive properties and provide tuning mechanisms [4, 5]. One recent report uses active electronics to tune a passive speaker, which serves as an acoustic absorber [6]. Typically, passive techniques are employed for mid to high frequency disturbances. At low frequencies, however, these techniques become bulky and heavy, thus making them undesirable. For these situations, active controllers can be more practical.

There are many considerations for implementing active noise control (ANC) [8]. Foremost is the control topology: feedforward vs. feedback. In feedforward control, "anti-noise" signals are created which can completely control plane waves or notch out zones of silence in harmonic, 3-dimensional sound fields. For this topology, a sensor, such as a microphone or accelerometer, is placed downstream from the disturbance source. This signal is then used to drive an electronic controller, typically an adaptive filter network, which is fed to an electormechanical transducer further downstream. Another sensor is incorporated in

feedforward design to measure the error at the control point and is used it improve the controller's performance. The first work in feedforward noise control dates to 1934 when Paul Lueg first proposed using interference sound waves to control noise in rigid walled ducts and tubes [8].

Often adaptive feedforward algorithms, which are implemented using digital finite impulse response (FIR) filters and digital signal processing (DSP) boards, are required along with some form of system identification. Such algorithms typically employ an iterative process that gradually generates new sets of FIR coefficients at every iteration so that the mean-squared error in the zone of silence is reduced over time. One popular example of this method is the least-mean-square algorithm, or LMS, which is based on a gradient descent algorithm. Updating the filter coefficients, however, is often computationally intensive. Therefore, works such as Douglas [10] have proposed algorithms, where the coefficients are only partially updated at every sample time, thus reducing the complexity of the overall system, up to 50%, when compared to a standard LMS controller. This makes these fast algorithms much more suitable for real time applications. Another recent feedforward method has utilized fuzzy logic for controlling a distributed source of broadband noise [11].

The second topology used in ANC is feedback control. For this method, a disturbance pressure field is detected by using a sensor microphone, which is used as an input to an electronic controller that conditions the magnitude and phase of the signal. The controller's output is then amplified and converted to an output pressure field at the sensor microphone. This conditioned "control" signal is then added to the disturbance field. These controllers have been used to create zones of silence using servo control [12] or to augment the dynamics (i.e. add damping) of an enclosed sound field. Implementations range from dissipative output feedback to robust and optimal model-based control designs [8]. Acoustic feeback control has a limited bandwidth because of the transducer dynamics and the time delay between the sensor and actuator.

For these reasons, this topology is far less popular in ANC than feedforward designs. In enclosed sound fields, these problems are compounded by high modal density of the enclosure and thus feedback control is seldom used in such circumstances [9]. However, there are cases where controlling a few modes is beneficial, such as ducts or mufflers or for

controlling transmission loss in finite structures [13, 14, 19, 20]. Control of low-frequency acoustic modes proves to be important for protecting payloads in launch vehicles. In these situations, the complications described above must be taken into consideration.

Feedback control of structural and acoustic systems are very similar while also having important differences. For example, unlike for structures, perfectly collocated sensor (microphone) and actuator (loudspeaker) pairs can not be achieved since the spatial aperture of the two transducers differ. By centering the microphone at the face of the loudspeaker, a "substantially collocated" transducer pair is achieved. However, unlike piezoceramic actuators used in structural control problems, the loudspeaker has significant dynamics which can be destabilizing and therefore erode controller performance. One report indicated that a 10% phase shift can reduce control effectiveness by 70% [25]. Several methods have been deduced which compensate for loudspeaker dynamics, two of which are described here.

One method for overcoming the effects of transducer dynamics in acoustic systems is to created a band-limited volume-velocity source, which was also used to demonstrate dissipative feedback control. In this procedure, the motion (either position, velocity, or acceleration) of the cone is measured and negatively fed back to the input voltage. By doing so, the poles, thus dynamics, are moved further to the left in the complex plane, thereby yielding nearly constant phase and magnitude response in low frequency regions. One issue with this technique, however, is that by adding the feedback loop, the overall gain of the loudspeaker is greatly reduced [15].

A second method was proposed to eliminate the loudspeaker dynamics in systems that have strong pressure coupling with the plant. However, in this case, the procedure described above is not as effective, since it only takes into account the internal dynamics of the loudspeaker. To address this problem, a velocity sensor which takes into account both the secondary coil voltage due to the motion of the loudspeaker cone and the primary coil current can be developed and used in conjunction with a proportional feedback controller. Doing so can result in an actuator that obtains nearly flat magnitude and phase response in the $20 - 200\,Hz$ frequency range [16].

An example of a relatively simple, yet effective structural feedback control approach is positive position feedback (PPF) [17]. In PPF, a control sensor and actuator that are

essentially free of dynamics at low frequencies (e.g., piezoceramic patches) are selected and collocated, which ensures that the control path is minimum phase. A simple block diagram of a PPF controller is given in Figure 1.

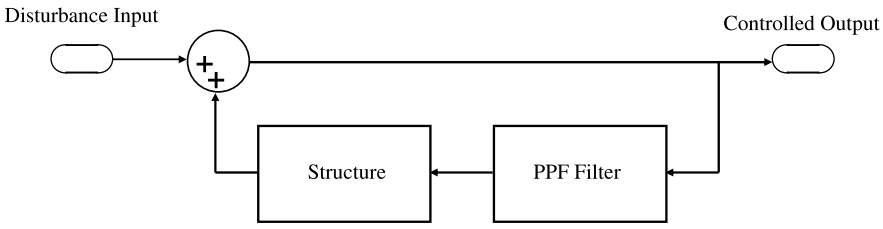

Figure 1: Block diagram of PPF controller.

The control signal is formed by feeding back structural displacement signals through a damped, resonant low-pass filter that is tuned to the desired structural resonance frequency [17, 18]. For a collocated sensor/actuator configuration, both the structure and low-pass filter each provide -90^o of phase at the desired resonant frequency. This is illustrated in Figure 2, where the response of a single mode structure and a PPF filter tuned to the structure's resonant frequency are plotted together.

Note, that typically the PPF filter's damping ration is selection to be at least ten times that of the structure to prevent an observable mode from being introduced in the closed-loop system. Since phase adds in series, the response of structure and the PPF filter together provides 180^o of phase at the control frequency. This signal is then positively fed back to the disturbance input signal, thus providing a cancelling effect. This behavior is seen in Figure 3, where the response of a structural disturbance signal (solid line), the series connection of the duct and PPF filter (dash-dotted line), and the controlled signal (dashed line) are given.

From Figure 3, it is seen that structure and filter do combine to provide the required 180^o of phase at the resonant frequency. Also, the closed-loop response has greatly reduced the structural disturbance signal. The advantages of this approach include the ability to selectively target any number of particular modes, it can be easily adapted electronically, and there are stability guarantees that can be met for structural control.

In the acoustic world, such an approach is considered to be similar to an active Helmholtz resonator. In the proposed active version, though, both the gain and the damping are much

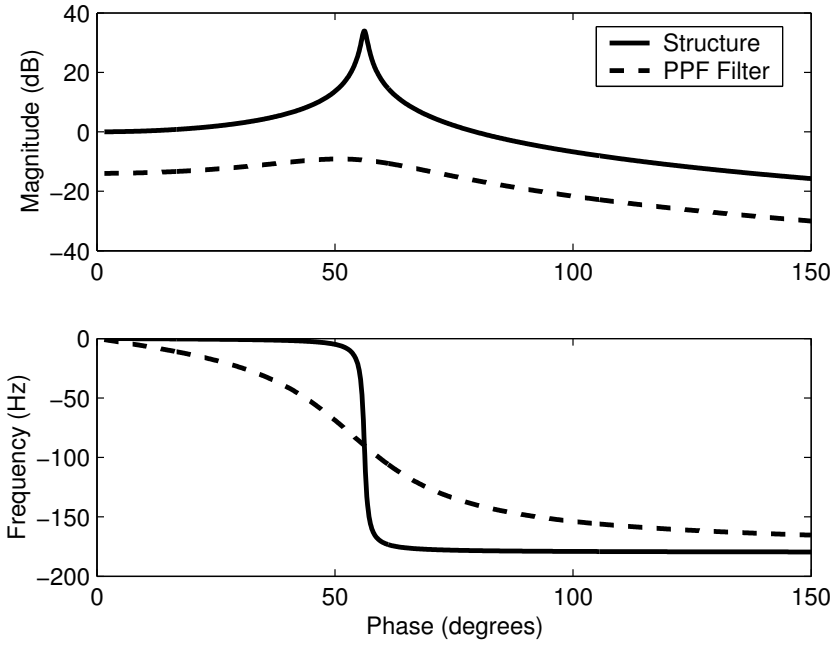

Figure 2: Response of a single mode structure and PPF filter.

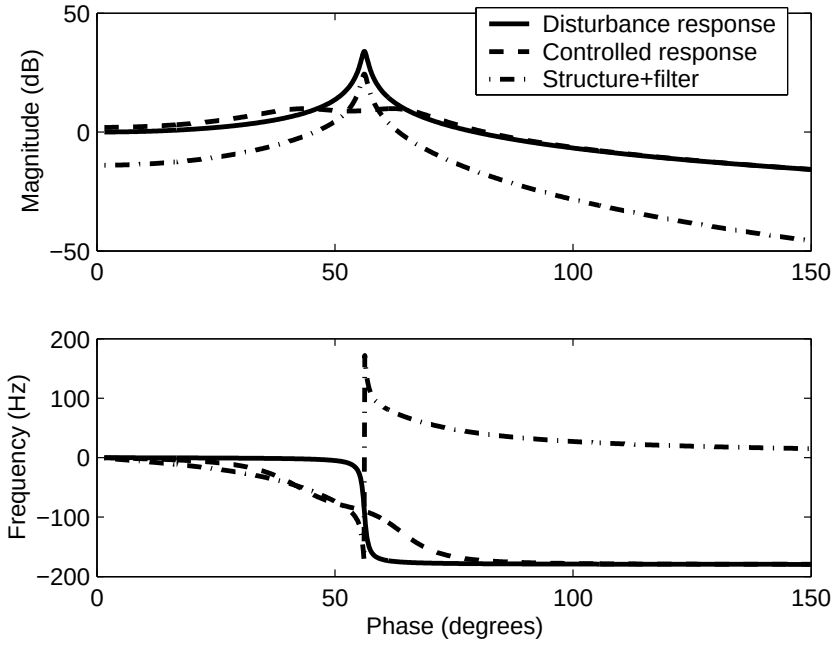

Figure 3: Disturbance/Controlled response for a single mode structure.

higher than for the passive counterpart. There is one report [26] that demonstrated PPF for acoustic control. By only targeting modes at frequencies above the loudspeaker's dynamics, its dynamics were neglected. This paper develops the theory for an active noise control device similar to PPF that includes a method to compensate the phase response of the loudspeaker actuator, thereby, permitting control in frequency regions where the loudspeaker dynamics are dominant. Although previously referred to as an "actively tuned acoustic absorber" [21], it will hence be referred to as an active noise absorber (ANA), to differentiate it from passive absorbers that are actively tuned [4, 5, 16]. A method to correct phase and provide performance and stability improvements will be presented, along with stability analysis using root locus techniques.

First, a theoretical model of a duct/loudspeaker system is developed. Next,control of the first two duct modes is demonstrated. Unlike Farinholt [26], where only non-inverting low-pass filters were utilized, this work does not place limitations on the chosen filter. Rather, gross phase compensation ($\pm$ 90°) of the loudspeaker dynamics is achieved by choosing either an inverting or non-inverting low-pass or band-pass resonant filter. It will also be shown that the bandpass provides more optimal magnitude response and thus will be favored. Instead of utilizing one of the above techniques which eliminate phase dynamics of the loudspeaker, here fine phase adjustments at the control frequency are accomplished by including an all-pass filter in the control-path. Once this technique is demonstrated with resonant 2^{nd}-order filters, the design is extended to utilize 4^{th}-order Butterworth bandpass filters, which are used to develop a multimodal controller. A previous publication of this study [27] focused only on collocated sensor/actuator pairs. This thesis will also consider the use of non-collocated choices, which is a benefit of using the all-pass filter. Finally, two companion experimental studies are provided that demonstrate control using a resonant filter over the fundamental duct mode and also demonstrates multimodal control in the fundamental and second duct modes.

2.0 MODELING THE SYSTEM

2.1 ANALYTICAL MODEL

The purpose of this study is to measure the impact of the feedback active noise control device on low frequency modes of an acoustic duct. For this study, a one-dimensional acoustic enclosure of length l_d, width w_d, and height h_d was chosen as a test bed. This plant was selected because of it provides a system with relatively sparse modal spacing, thus allowing the study of the first few modes. This rigid-walled duct has two enclosed midrange loudspeakers of face width w_s. One is centered at x_1 that provides the disturbance input and the other, centered at x_2, serves as the control actuator. Also included is the coordinate of an error sensor, x_e, which will be discussed later. A schematic of this setup can be found in Figure 4.

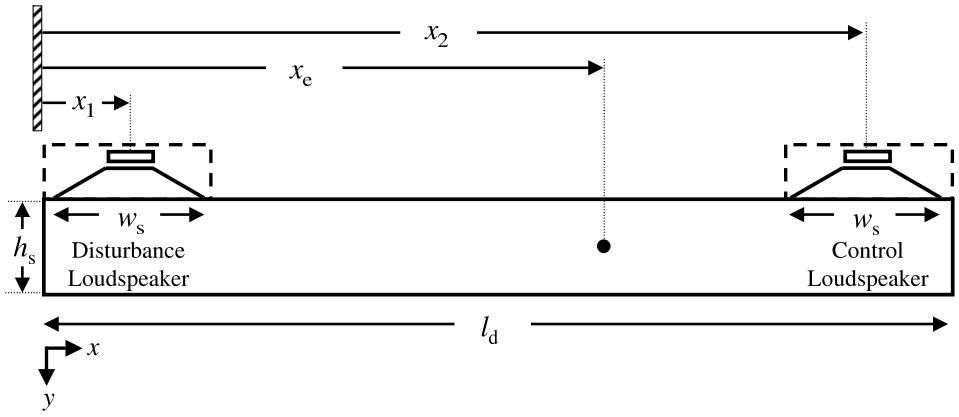

Figure 4: Rigid walled acoustic duct setup.

An analytical model describing the plant will now be developed that is consistent with an experimental test bed in the Sound, Systems, and Structures Laboratory at the University of

Pittsburgh. In the following sections, the governing equations for the midrange loudspeakers and the acoustic duct will be presented. For a more detailed derivation of these equations see Fahy [22].

2.1.1 Acoustic Duct

To model the duct, the inhomogeneous wave equation, in terms of pressure, is used. The general form of the equation can be written as

$$\nabla^2 p(x,t) - \frac{1}{c^2}\frac{\partial^2 p(x,t)}{\partial t^2} = \rho_o \sum_{j=1}^{J} \frac{\partial^2 y_j(t)}{\partial t^2}, \; n = 1 \ldots \infty, \tag{2.1}$$

where $p(x,t)$ is the time dependent acoustic pressure at a point x inside the duct; c is the speed of sound in air; and ρ_o is the air density. In addition, the speaker is modeled as a piston where $y_j(t)$ is the displacement function of the j^{th} speaker. The acoustic response of the duct can be represented in modal coordinates as

$$p(x,t) = \sum_{n=1}^{\infty} p_n(t)\Psi_n(x), \tag{2.2}$$

where p_n and Ψ_n are the n^{th} pressure mode and eigenfunction of the enclosure respectively [22]. By applying the closed-closed boundary conditions and a volume normalization, Ψ_n is written as

$$\Psi_n = \frac{2}{l_d}\cos\left(\frac{n\pi x}{l_d}\right), \tag{2.3}$$

where x is an arbitrary point inside the duct. Applying the orthogonality condition and substituting Equations (2.3) and (2.2) into (2.1) and integrating the resulting equation over the fluid volume, the duct pressure in modal coordinates becomes

$$\ddot{p_n} + \omega_n^2 p_n = \rho_o c^2 \sum_{j=1}^{J} \int_{A_j} \Psi_n(x_j)\ddot{y_j}\, dA, \tag{2.4}$$

where

$$\omega_n = \frac{n\pi c}{l_d} \tag{2.5}$$

is the natural frequency of the n^{th} duct pressure mode and A_j is the area of the j^{th} loudspeaker. By assuming the speaker's cross sectional area can be treated as as square, the right hand side of Equation (2.4) can now be written as

$$\frac{2\rho_o c^2 \mathrm{w}_s}{l_d} \sum_{j=1}^{2} \int_{x_{j1}}^{x_{j2}} \Psi_n(x_j) \ddot{y_j}\, dx, \tag{2.6}$$

where w_s is the speaker face width and x_{j1} and x_{j2} indicate the left and right edges of the disturbance ($j = 1$) and control ($j = 2$) loudspeaker, respectively. Performing the integration in Equation (2.6) and substituting Equation (2.3) into the result gives the final governing equation for the duct

$$\ddot{p_n} + \zeta_d \omega_n \dot{p_n} + \omega_n^2 p_n = \frac{2\rho_o c^2 A}{l_d} \sum_{j=1}^{2} \ddot{y_j} \phi_j, \tag{2.7}$$

where

$$\phi_j(n) = \frac{2\mathrm{w}_s}{n\pi A} \left[\sin\left(\frac{n\pi x_{j2}}{l_d}\right) - \sin\left(\frac{n\pi x_{j1}}{l_d}\right) \right], \; n = 1 \ldots N, \; j = 1, 2. \tag{2.8}$$

Equation (2.7) also includes the duct damping ratio, ζ_d. This is introduced to represent the internal dissipation and to properly bound the model. Notice that the infinite summation over n is truncated to N, where N is large enough for the model to converge over the bandwidth of interest. The one-dimensional model is valid if the applied system is operated below the lowest cutoff frequency, f_{co} [7]. For the experimental setup in question, the cutoff frequency can be calculated by

$$f_{co} = \frac{c}{2\mathrm{w}_d} = \frac{343}{.3302\, s} = 1039 Hz. \tag{2.9}$$

Thus, Equation (2.7) provides a set of uncoupled equations that completely describe the low frequency behavior of the duct.

2.1.2 Loudspeakers

The next step is to develop the mathematical models for the loudspeakers. As shown in Figure 4, both the acoustic disturbance signal and the control signal excite the duct via midrange loudspeakers. A generic schematic for a cone speaker is provided in Figure 5.

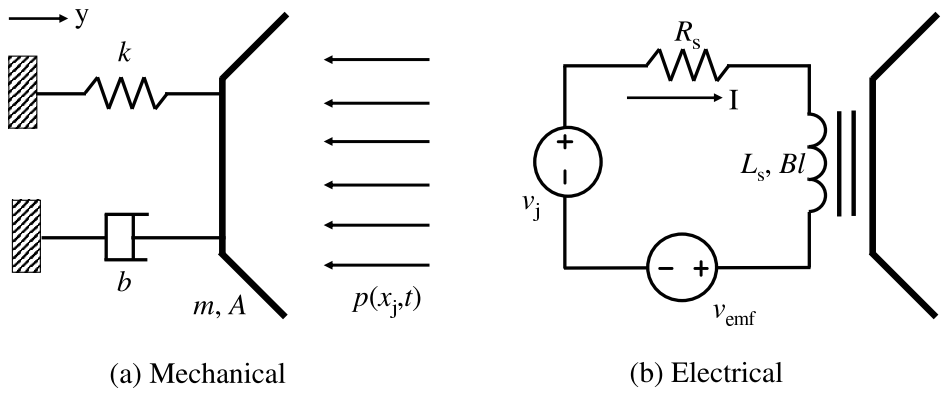

Figure 5: Loudspeaker schematic.

The two inputs for each loudspeaker include the pressure acting on the speaker face and the voltage to the coil; the output is the acceleration of the speaker cone, which acoustically excites the duct. Since loudspeakers are coupled electro-mechanical systems, two differential equations are needed to describe their behavior. The mechanical equation of motion for both of the loudspeakers, (Figure 5(a)) is

$$\ddot{y_j} + \frac{b}{m}\dot{y_j} + \frac{k}{m}y_j = \frac{Bl}{m}I_j - \frac{A}{m}p(x_j, t), \tag{2.10}$$

where m and A are the the mass and cross sectional area of the loudspeaker cone, and b and k are the damping ratios and the stiffness of the loudspeaker respectively. The input pressure, which acts on the cone area, is given by $p(x_j, t)$ and the electro-mechanical coupling, which creates an applied force that opposes the input pressure, is given by the product of the Bl constant and the current through the coil, I_j.

Using the acoustic/mechanical coupling given in (2.8) along with Equations (2.2) and (2.3), the modal form of Equation (2.10) can be written as

$$\ddot{y}_j + \frac{b}{m}\dot{y}_j + \frac{k}{m}y_j = \frac{Bl}{m}I_j - \frac{A}{m}\sum_{n=1}^{N} p_n(t)\phi_j, \;\; j = 1, 2. \tag{2.11}$$

To complete the mathematical representation, the electrical equation must also be included. By summing the voltages around the loop in Figure 5(b), the equation that describes the electrical behavior is given by

$$\dot{I}_j + \frac{R_s}{L_s}I_j = \frac{v_j(t)}{L_s} - \frac{Bl}{L_s}\dot{y}_j, \;\; j = 1, 2, \tag{2.12}$$

where, L_s and R_s are the internal inductance and resistance of the loudspeaker and $v_j(t)$ is the input voltage. In this case, the Bl term produces a voltage in proportion to the loudspeaker voice coil velocity ($v_{emf} = Bl\dot{y}_j$), which opposes the applied voltage.

2.2 STATE SPACE REPRESENTATION AND MODEL VERIFICATION

The above governing equations (2.7, 2.11, 2.12) can now be used to derive a state space model to describe the experimental setup (less control speaker for uncontrolled case). However, it is first necessary to present the system topology in order to determine the inputs and outputs of the plant. A schematic showing the chosen plant topology, is seen in Figure 6.

The duct model shown in Figure 6 includes two acceleration inputs: $\ddot{y}_1$ is the acceleration from the disturbance loudspeaker, which is considered to be a component of the uncontrolled plant system, while $\ddot{y}_2$ is the acceleration output from the acoustic controller, which will be discussed in detail later. The duct is also developed to include four outputs. The first and last outputs, $F(x_1, t)$ and $F(x_2, t)$, are the integrated forces acting on the disturbance and control loudspeakers, respectively. The second output, $p(x_e, t)$, represents the point error pressure response at position x_e, and can be set to record any point within the duct. The final output, $p(x_{sen}, t)$ is the point sensor pressure for the controller and is set to $x_{sen} = x_2$ for a substantially colocated sensor/actuator pair. Notice that the block diagram for the duct has been partitioned into two sections: one designated the disturbance duct, which

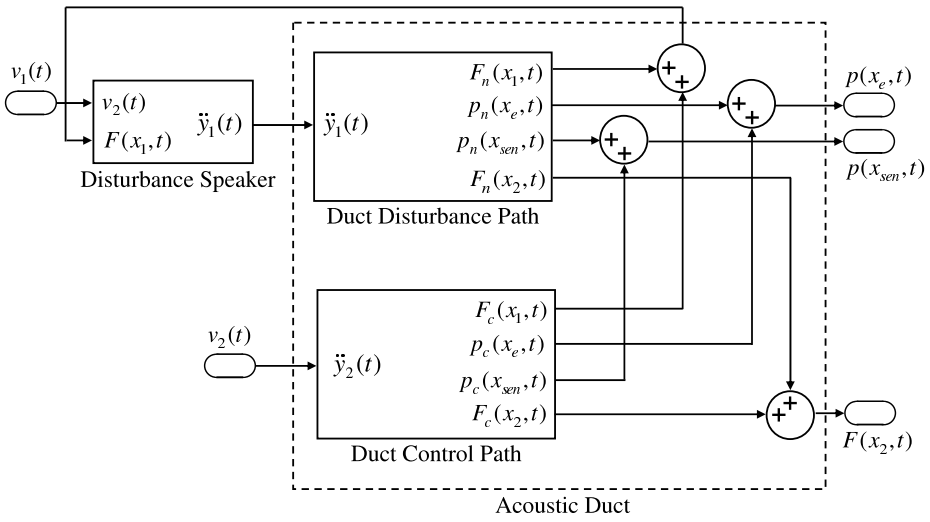

Figure 6: Plant schematic showing system conventions.

takes $\ddot{y}_1$ as an input; and the other, called the control duct, which accepts $\ddot{y}_2$ as an input. Each of the four outputs, therefore, consists of the of the summation of the output responses due to each of the partitioned segments. The subscripts of n and c are used to represent the outputs that result from the disturbance duct and the control duct, respectively.

In the following sections, the state-space models for both the duct and the loudspeaker will be presented. The generic state equations can be written as

$$\{\dot{\mu}\} = \mathbf{A}\{\mu\} + \mathbf{B}\{U\} \tag{2.13}$$

and

$$\{\varphi\} = \mathbf{C}\{\mu\} + \mathbf{D}\{U\}, \tag{2.14}$$

where μ is a state variable, $\mathbf{A}$ is the dynamics matrix, $\mathbf{B}$ is the input matrix, U is the input vector, φ is the output vector, $\mathbf{C}$ is the output matrix, and $\mathbf{D}$ is the feedthrough matrx. This form was chosen, as opposed to a transfer function representation, because it yields a form that is more natural to work with when using the MATLAB$^{\text{TM}}$ software package. When the derivations are complete, the results of a fully coupled simulation will be given and verified against data taken from the experimental test bed.

2.2.1 Acoustic Duct State Matrices

To begin the developement of the duct model, consider Equation (2.7), which provides the information regarding the inputs and the internal dynamics of the duct and Equations (2.2) and (2.3), which will provide the information regarding the outputs of the duct. For the system shown in Figure 6, the inputs to the duct will consist of the two accelerations from each of the loudspeakers and the outputs of the duct will be two point pressures and two distributed forces.

This set of equations can be used to derive the $\mathbf{A_d}$ matrix and the $\mathbf{B_d}$ matrices of the state-space model. However, to alleviate the derivation, some simplifications in notation are first presented. The first simplification is made by combining the constant terms on the right side of Equation (2.7) with equation (2.8). This combination, which is called $\beta_j(n)$ can be written as

$$\beta_j(n) = \frac{2\rho_o c^2}{l_d}\phi_j(n), \;\; j = 1, 2. \tag{2.15}$$

Second, since the acceleration terms are the input variables, the $\ddot{y_j}$ notation can be dropped in favor of the more conventional U_j notation. Finally, as stated in the previous chapter, the number of the modes can be truncated to a finite number, N, such that N is large enough to guarantee convergence to the experimental response. Making these substitutions and solving for the highest derivative, Equation (2.7) now becomes

$$\ddot{p_n} = -\zeta\omega_n\dot{p_n} - \omega_n^2 p_n + \beta_1(n)U_1 + \beta_2(n)U_2, \;\; n = 1 \ldots N. \tag{2.16}$$

By examining Equation (2.16), it is seen that the $\mathbf{A_d}$ matrix will have dimensions $(2N)$x$(2N)$, which indicate that there is a total of $2N$ states. These states are ordered so that the odd states represent modal pressures and the even states represent their derivatives. Thus, $\mu_{2*n-1} = p_n$ and $\mu_{2*n} = \dot{p_n}$. Using these state choices along with Equation (2.16), the two relavent equations needed to form the $\mathbf{A_d}$ matrix are

$$\dot{\mu}_{2*n-1} = \mu_{2*n} \tag{2.17}$$

and

$$\dot{\mu}_{2*n} = -\omega_n^2 \mu_{2*n-1} - \zeta\omega_n \mu_{2*n} + \beta_1(n)U_1 + \beta_2(n)U_2. \tag{2.18}$$

Now Equations (2.17) and (2.18) are combined to yield the $\mathbf{A_d}$ maxtrix, which is shown to be

$$\mathbf{A_d} = \begin{bmatrix} 0 & 1 & 0 & 0 & 0 & \cdots & 0 & 0 \\ -\omega_1^2 & -2\zeta\omega_1 & 0 & 0 & 0 & \cdots & 0 & 0 \\ 0 & 0 & 0 & 1 & 0 & \cdots & 0 & 0 \\ 0 & -\omega_2^2 & -2\zeta\omega_2 & 0 & 0 & \cdots & 0 & 0 \\ \vdots & \vdots & \vdots & \vdots & \vdots & \ddots & \vdots & \vdots \\ 0 & 0 & 0 & 0 & 0 & \cdots & 0 & 1 \\ 0 & 0 & 0 & 0 & 0 & \cdots & -\omega_N^2 & -2\zeta\omega_N \end{bmatrix}. \tag{2.19}$$

Since there are N states and two inputs, the $\mathbf{B_d}$ matrix will have dimensions $(2N)$x2. From Equation (2.18), it is seen that the $\beta_1(n)$ terms multiply the U_1 input with these terms making up the first column of the $\mathbf{B_d}$ matrix. Likewise, the $\beta_2(n)$ terms multiply the second input, U_2, thus making up the second column. Because the coefficients of Equation (2.16) only exist on even numbered rows of the $\mathbf{A_d}$ matrix, odd rows of the $\mathbf{B_d}$ matrix will be null. This can be written as

$$\mathbf{B_d} = \begin{bmatrix} 0 & \beta_1(1) & 0 & \beta_1(2) & \dots & 0 & \beta_1(N) \\ 0 & \beta_2(1) & 0 & \beta_2(2) & \dots & 0 & \beta_2(N) \end{bmatrix}^T. \tag{2.20}$$

Now that the $\mathbf{A_d}$ and $\mathbf{B_d}$ matrices are derived, focus can be directed towards the output $\mathbf{C_d}$ matrix. To begin its derivation, consider the second and third outputs from Figure 6. The equation describing these point pressure taps is found by combining Equations (2.2) and (2.3) as such

$$p(x_{e,sen}, t) = \frac{2}{l_d} \sum_{n=1}^{N} p_n(t) \cos\left(\frac{n\pi x}{l_d}\right), \tag{2.21}$$

where x_e and x_{sen} are the locations of the error pressure and the sensor pressure respectively. As was done above, two simplifications in notation can be made. The first of these is made by letting

$$\gamma(n, x_{e,\,sen}) = \frac{2\cos\left(\frac{n\pi x}{l_d}\right)}{l_d}, \tag{2.22}$$

and the second is made by replacing $p_n(t)$ with its relevant state variable, μ_{2*n-1}. By substituting these simplifications into Equation (2.21), the equation describing the second and third outputs of the duct is written as

$$p(x_{e,\,sen}, t) = \sum_{n=1}^{N} \mu_{2*n-1}\gamma(n, x). \tag{2.23}$$

Since the first and last outputs are not point pressures, but rather distributed forces acting on the faces of the two loudspeakers, information regarding these outputs is taken from the second term on the right side of Equation (2.11). Making similar simplifications as was done in Equation (2.23), the output equation is written as

$$F(x_j, t) = A\phi_j(n)\mu_{2*n-1},\ \ j = 1 \ldots 2. \tag{2.24}$$

Since there are four outputs and N states, the dimensions of the $\mathbf{C_d}$ matrix is 4 x $(2N)$. Ordering the rows in the same manner that is shown in Figure 6, the $\mathbf{C_d}$ matrix can be written as such

$$\mathbf{C_d} = \begin{bmatrix} A\phi_1(1) & 0 & A\phi_1(2) & 0 & \cdots & A\phi_1(N) & 0 \\ \gamma(1, x_e) & 0 & \gamma(2, x_e) & 0 & \cdots & \gamma(N, x_e) & 0 \\ \gamma(1, x_{sen}) & 0 & \gamma(2, x_{sen}) & 0 & \cdots & \gamma(N, x_{sen}) & 0 \\ A\phi_2(1) & 0 & A\phi_2(1) & 0 & \cdots & A\phi_2(1) & 0 \end{bmatrix} \tag{2.25}$$

Finally, the $\mathbf{D_d}$ matrix is presented. Since no feedthrough is needed for the duct, the $\mathbf{D}$ matrix will be the 4 x 2 zero matrix. For completeness, this is shown to be

$$\mathbf{D_d} = \begin{bmatrix} 0 & 0 & 0 & 0 \\ 0 & 0 & 0 & 0 \end{bmatrix}^T. \tag{2.26}$$

The four state matrices presented above can be substituted into Equations (2.13) and (2.14) to form the final state-space model describing the duct, which will be used for simulation purposes. In the next section, the same process will be used to form the state matrices for the two loudspeakers.

2.2.2 Loudspeaker State Matrices

Because the loudspeakers are descibed by a second-order mechanical equation given by equation (2.11) and a single-order electrical given by equation (2.12), only three states are required. For this system, let $\mu_1 = I_j$, $\mu_2 = y_j$ and $\mu_3 = \dot{y}_j$. Solving these two equations for their highest derivatives and making these substitutions results in the following set of equations:

$$\dot{\mu_1} = -\frac{R_s}{L_s}\mu_1 - \frac{Bl}{L_s}\mu_3 + \frac{1}{L_s}V_{in} \tag{2.27}$$

$$\dot{\mu_3} = \frac{Bl}{m}\mu_1 - \frac{k}{m}\mu_2 - \frac{b}{m}\mu_3 - \frac{1}{m}F(x_j, t) \tag{2.28}$$

Notice that the loudspeaker area, A, has been omitted from Equation (2.11) to reflect the force input as opposed to pressure. Using these two equations, and setting $\dot{\mu_2} = \mu_3$, the $\mathbf{A_s}$ and $\mathbf{B_s}$ matricies may be written as:

$$\mathbf{A_s} = \begin{bmatrix} -R_s/L_s & 0 & -Bl/L_s \\ 0 & 0 & 1 \\ Bl/m & -k/m & -b/m \end{bmatrix}, \ \mathbf{B_s} = \begin{bmatrix} 0 & 1/L_s \\ 0 & 0 \\ 0 & -1/m \end{bmatrix} \tag{2.29}$$

In order to obtain the output relation for the loudspeaker, Equation (2.28) is utilized. Since the acceleration output is the derivative of μ_3, the feedthrough matrix is needed, Thus, the $\mathbf{C_s}$ and $\mathbf{D_s}$ matrices are shown to be:

$$\mathbf{C_s} = \begin{bmatrix} Bl/m & -k/m & -b/m \end{bmatrix}, \ \mathbf{D_s} = \begin{bmatrix} 0 & -A_s/m \end{bmatrix} \tag{2.30}$$

As before, the resulting matricies can be substituted into Equations (2.13) and (2.14) to form the state-space model describing the loudspeakers. Using the duct and loudspeaker

models, a simulation of the coupled plant is now presented and verified against data taken from the experimental test bed.

2.3 SIMULATED PLANT RESPONSE AND MODEL VERIFICATION

The plant model was assembled and simulated in MATLAB^{TM} using the state-space representations of the duct and speaker models derived in the previous sections. To be consistent with the experimental test bed, the internal dimensions of the duct and the parameters for the Peerless 832592 loudspeakers are used in the simulation. These values, along with the properties of air, are listed in Table 1. The MATLAB^{TM} code pertaining to the duct is presented in Appendix A, and code for the loudspeaker is presented in Appendix B.

In order to verify the MATLAB^{TM} model, the analytical frequency response between $v_1(t)$ and $p(x_e, t)$ with x_e set to x_2 is plotted against measured results from the test bed as shown in Figure 7. This response consists of the combination of the disturbance loudspeaker and the duct disturbance-path, but will be referred to simply as the disturbance-path. Through a trial and error approach, the low-frequency model from $0 - 500\,Hz$ is found to converge with $N \geq 36$, and thus $N = 40$ is chosen.

It is seen that the simulated results predict the behavior of the experimental test bed reasonably well. The discrepancy in the analytical model with the experimental data will not inhibit the development of a design procedure for an ANA controller. Thus focus is now directed to developing a compensator that will selectively control one of the duct modes observed in Figure 7.

Table 1: Plant parameters used in simulation.

Duct		*Loudspeaker*	
Param.	Value	Param.	Value
l_d	$3.0\,m$	A	$85.0\,cm^2$
w_d	$16.5\,cm$	b	$1.30\,Ns/m$
h_d	$16.5\,cm$	k	$12.5\,kN/m$
w_s	$9.22\,cm$	m	$7.8\,g$
x_1	$0.1\,m$	Bl	$5.5\,N/A$
x_2	$2.9\,m$	L_s	$1.1\,mH$
ρ_o	$1.23\,kg/m^3$	R_s	$6.1\,\Omega$
c	$346\,m/s$	-	-

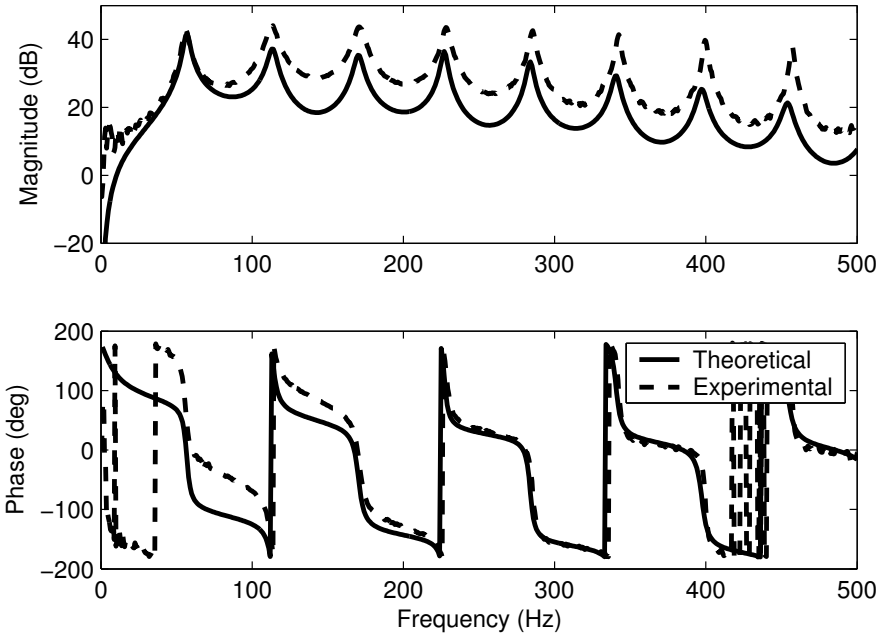

Figure 7: Simulated and experimental results for disturbance-path.

3.0 COMPENSATOR DESIGN

In this chapter, a design process is developed that will target and control one of the duct modes shown in Figure 7. To perform this control, a device called an active noise absorber (ANA) similar to ones used for structural PPF [17], is designed and used to control the acoustic pressure modes. The controller uses a reference pressure as an input and feeds back an output pressure to the duct. As with structural PPF, described in [17, 18], both a collocated sensor/actuator pair and a tuned 2^{nd}-order filter are initially used to generate an output signal that is perfectly out of phase (180^o) with the input at the desired control frequency, ω_c. Unlike the structural PPF examples [17, 18], however, the dynamics of the acoustic loudspeaker will add phase to the control path, which affects the performance and stability of the closed-loop system. To produce the required 180^o of phase, these added dynamics must be accounted for.

Once the procedure is shown using resonant 2^{nd}-order filters, the design will be then extended to use 4^{th}-order Butterworth band-pass filters. It will also be shown that the phase compensation technique has the added benefit of allowing the use of non-collocated sensor/actuator pairs. Finally, a multimodal case is illustrated where control over the fundamental and second duct mode is achieved.

3.1 FEEDBACK CONFIGURATION

First consider the block diagram of the closed-loop system shown in Figure 8. From this, it is seen that the control-path of the system contains a filter network, which consists of a sensor microphone that measures $p(x_{sen}, t)$, a damped resonant filter, and a phase compensation

filter; a control speaker; and the duct transfer function between $\ddot{y}_2$ and $p(x_{sen}, t)$, where x_{sen} is collocated with x_2 and thus $\ddot{y}_2$.

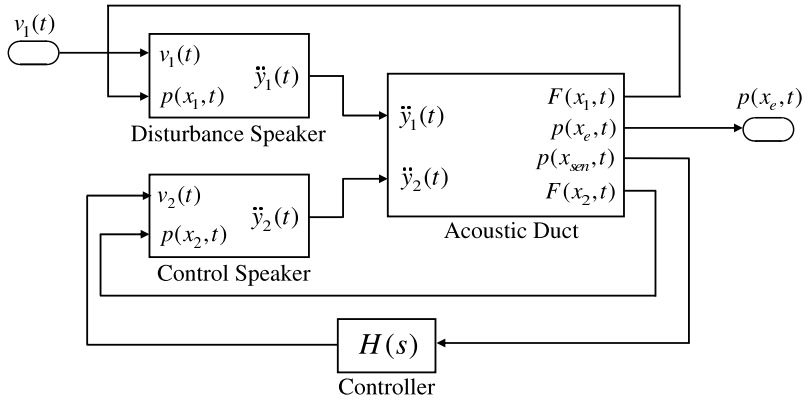

Figure 8: Closed-loop system schematic.

In order to gain more insight into the controller's topology, which will aide in the design of filter network, it is now advantageous to develop a simplified model of the controller cast in a feedback setting. In addition, many classical feedback techniques, such as root-locus analysis, may be utilized when the controller is in this form. With that being said, now consider the feedback diagram shown in Figure 9.

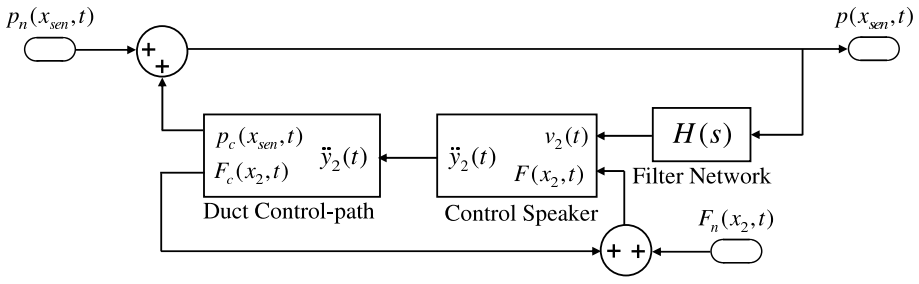

Figure 9: Fully coupled feedback model of controller.

The feedback model shown in Figure 9 uses $p_n(x_{sen}, t)$ from the duct disturbance path as an input, and outputs a total pressure, $p(x_{sen}, t)$. In this configuration, the effects of the force coupling between the control loudspeaker and the duct can be observed. Part of the

input force acting on the control loudspeaker cone is due to back coupling from the duct control-path, $F_c(x_2, t)$, while the remainder, $F_n(x_2, t)$, is due to the influence of the duct disturbance-path. The latter force is unwanted and may be treated as a noise input to the control-path. It was found that ignoring this force produced only minor errors in the overall design of the controller. Also, the reduced model allows for easy calculation of the stability range using either root locus or the Nyquist Stability Criteria. This simplified model is shown in Figure 10.

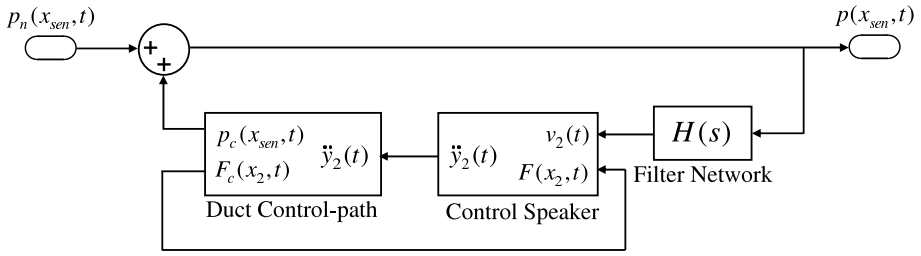

Figure 10: Simplified feedback model of controller.

3.2 RESONANT FILTER DESIGN

In this section, the resonant 2^{nd}-order filter component of the filter network, $H_c(s)$, will be designed. From Figure 10, it can be seen that the series connection of the duct, the filter network, and the loudspeaker each contribute phase, θ_c, to the control-path as

$$\theta_c(\omega_c) = \theta_f(\omega_c) + [\theta_s(\omega_c) + \theta_d(\omega_c)], \tag{3.1}$$

where θ_f is the phase of the compensation filter, θ_s is the phase of the loudspeaker, and θ_d is the phase of the duct control-path. Note, the terms in brackets indicate that the duct and loudspeaker are coupled, and thus, the phase response needs to be measured together for accurate results. It is desired that $\theta_c(\omega_c) = \pm 180^o$ for positive feedback control. Before discussing the design of the compensation filter, it is useful to first examine the overall magnitude and phase response of the control loudspeaker and duct control-path. The frequency

response functions of the duct, control loudspeaker, and their combination are plotted in Figure 11.

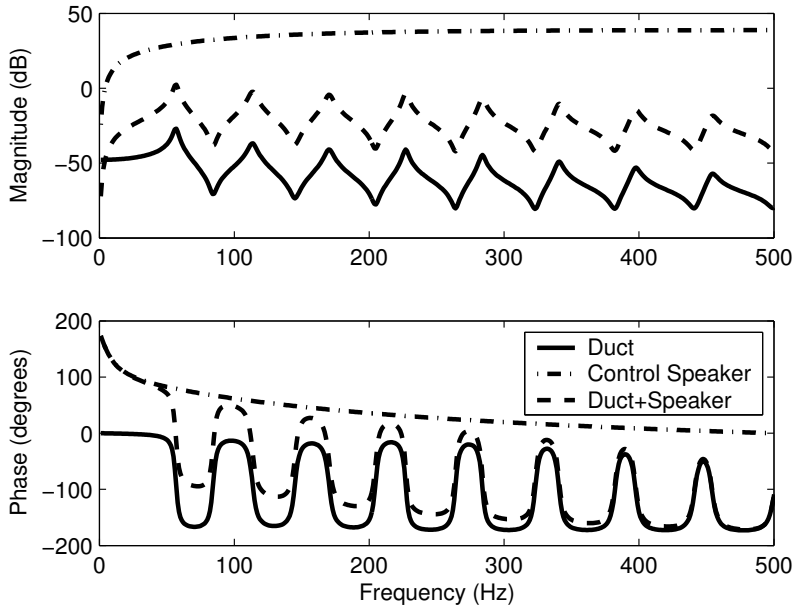

Figure 11: Frequency response of control speaker, duct, and duct+loudspeaker.

From the solid line in Figure 11, it is seen that the phase of the duct is always -90^o phase at the modal frequencies when the input and output are collocated. This is consistent with PPF where the structure always contributed -90^o at any of the resonant frequencies that are controlled. In contrast, the phase of the loudspeaker transfer function between v_2 and $\ddot{y_2}$, given by the dash-dot line, varies from $+180^o$ to approximately 0^o within the $500\,Hz$ frequency range under consideration. When this effect is combined with the duct, the phase response of the control-path, shown by the dashed line, at each resonance varies from roughly from 0^o to -90^o. For control, some form of fine phase-compensation needs to be added to correct this phase shift introduced by the loudspeaker so that the net phase response at the control frequency is $\pm 180^o$. The phase-compensation strategy will be presented in the next section.

For the gross phase and magnitude adjustment of the control-path shown in Figure 11, both low-pass, $H_{LP}(S)$, and band-pass, $H_{BP}(S)$, 2^{nd}-order filters are initially considered. Their respective transfer functions are given below

$$H_{LP}(S) = \frac{\pm G\omega_n^2}{s^2 + 2\zeta_c\omega_c s + \omega_n^2} \tag{3.2}$$

and

$$H_{BP}(S) = \frac{\pm G\omega_n s}{s^2 + 2\zeta_c\omega_c s + \omega_n^2}. \tag{3.3}$$

Here, ζ_c is the filter damping ratio and G is a gain which takes into account both the microphone and amplifier. Using each of these filters, the frequency response of the control-path with ω_c set to the first duct pressure mode of $56.6\,Hz$ is evaluated. The results of combining a first mode low-pass filter with the duct are seen in Figure 12(a) and results for the band-pass filter are seen in Figure 12(b).

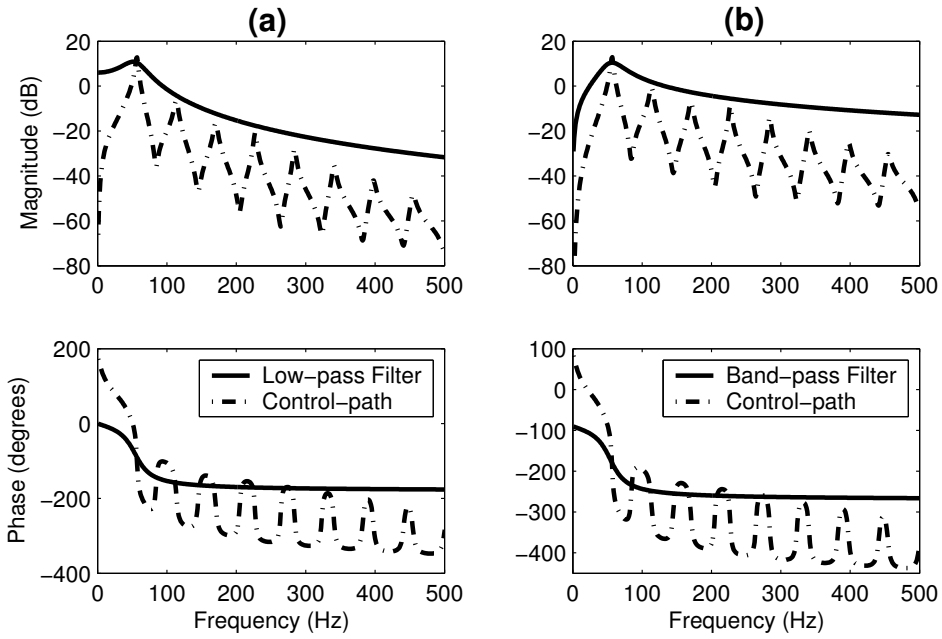

Figure 12: Frequency response of control-path and low/band-pass filter.

From Figure 12(a), it is observed that the low-pass filter yields little magnitude change to the control-path below f_c, but provides a roll-off of $40\,dB/dec$ above it. In addition to the

magnitude characteristics, the low-pass filter also contributes a phase adjustment of -90^o at the targeted mode: 90^o if inverting. In contrast, the band-pass filter seen in Figure 12(b) provides for attenuation in both the low and high frequency regions to either side of f_c. The high-frequency roll-off of $20\,dB/dec$, however, is slower than the low-pass filter. It is also seen that the phase adjustment of the band-pass filter at ω_c is 0^o: 180^o if inverting. These characteristics, in addition to the phase response of the loudspeaker determine the range of G before instability occurs at either modes above or below f_c.

The damping ratio and gain of the filters can have an impact on both performance and stability of the controller, primarily through the gain at f_c, and also by introducing an observable mode if $\zeta_c << 1.0$. To maintain stability, the maximum gain of any in-phase region (0^o) of the control-path must always be less than 1. This ensures the gain margin will be positive and is consistent with the Nyquist stability criteria.

3.2.1 Phase Compensation

As mentioned previously, the phase shift introduced by the loudspeaker, $\theta_s(\omega_c)$, can prevent the control-path phase, $\theta_c(\omega_c)$, in Equation (3.1) from being a multiple of 180^o. The resonant filters given by Equation (3.2) and (3.3) can only adjust the phase in 90^o multiples, and thus are used to provide a gross phase adjustment. There are, however, several possible methods for correcting the phase of the speaker. Examples include lead-lag compensation, building an approximate volume-velocity control loudspeaker [15], or using an all-pass phase-shaping circuit. Since both the volume velocity approach and lead-lag compensation may adversely impact the magnitude of the control loop, the all-pass filter is chosen. An all-pass filter has unity gain and can provide a phase shift ranging from $0-180^o$ if non-inverting, or $180-360^o$ if inverting. The transfer function of the all-pass filter is written as

$$H_{AP}(S) = \frac{\pm(s-z)}{s+p}, \tag{3.4}$$

where, z is the zero location of the all-pass filter and p is the pole location [23], where the pole and zero must be equal, $(z = p)$. Considering Figures 12(a) and 12(b), the desired

all-pass filter phase is chosen to be the supplemental angle of $\theta_c(\omega_c)$ as

$$\theta_a = 180 - \theta_c(\omega_c) = 180 - \{\theta_f(\omega_c) + [\theta_s(\omega_c) + \theta_d(\omega_c)]\}\,. \tag{3.5}$$

If $0 < \theta_a < 180$, then a non-inverting all-pass is used and the pole/zero location is calculated using

$$p = z = \frac{\omega_c}{\cot\left(\frac{\pi\theta_a}{360}\right)}. \tag{3.6}$$

However, if $180 < \theta_a < 360$, then an inverting all-pass is used and the pole/zero location is calculated using

$$p = z = -\frac{\omega_c}{\tan\left(\frac{\pi\theta_a}{360}\right)}. \tag{3.7}$$

Once the all-pass pole/zero is calculated, the filter is then added to the control-path to create a compensator that will produce a perfectly out-of-phase modal control signal. The following five-step algorithm summarizes the steps required to design the appropriate controller.

1. Determine the targeted mode of control.
2. Obtain the phase response of duct control-path and loudspeaker combination.
3. Choose the best filter to provide gross phase and magnitude compensation .
4. Obtain the phase response of the duct, controller, and resonant filter.
5. If the phase response is not within $\pm 2\%$ of 180^o, perform the following:
   - Use Equation (3.5) to find the required phase compensation, θ_a.
   - Calculate the all-pass filter pole using either Equation (3.6) if $0 < \theta_a < 180$, or Equation (3.7) if $180 < \theta_a < 360$.

3.2.2 Resonant Filter Control Simulation

A full controller is now developed and simulated using the techniques described above. First, consider the case where the loudspeaker is not present ($\theta_s = 0^o$) in the controller. Since $\theta_d = -90^o$, it is seen from Equation 3.1 that the required phase of the compensator is -90^o, which is realized with a non-inverting low-pass filter. Choosing the first pressure mode as the target of control, ω_c in Equation 3.2 is $356\,rad/s$ ($56.6\,Hz$). A filter gain of $G = 10.0$ and a damping ratio of $\zeta_c = 0.35$ are heuristically chosen for this step, however, a stability analysis

will be performed before the final controller is developed. Figure 13 shows the resulting disturbance-path/closed-loop response for a transfer function between x_1 and $p(x_e, t)$ with $x_e = x_2$. Also included is the control-path transfer function.

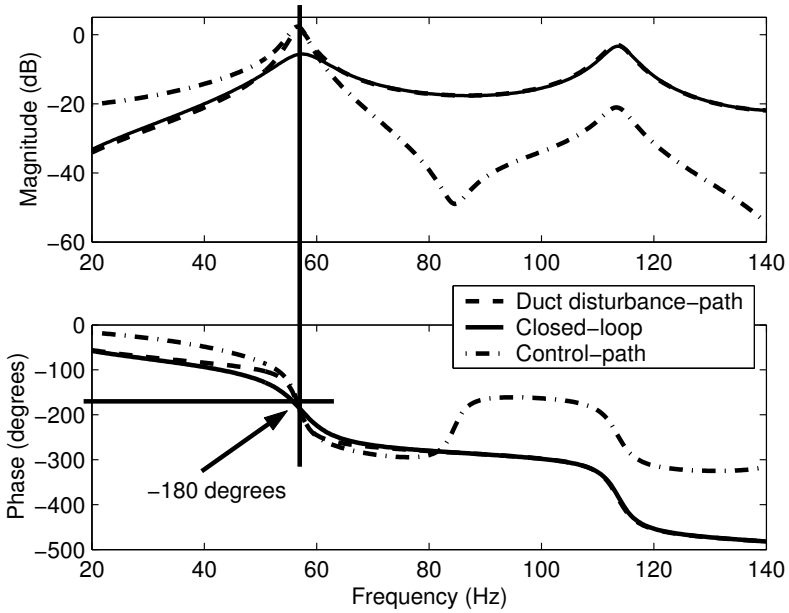

Figure 13: Predicted disturbance-path/closed-loop response without speaker dynamics.

Notice that the control-path frequency response, given by the dashed-dotted line, does indeed have -180^o phase at the first pressure mode ($f_1 = 56.6\,Hz$). Also, note that about $5\,dB$ of attenuation has been predicted when comparing the disturbance-path (dashed line) and closed-loop response (solid line), which are taken between the disturbance input, $v_1(t)$, and the error sensor, $x_e = x_2$. Now contrast these results with those given in Figure 14, where the loudspeaker dynamics are included. Note, that for this simulation, the filter gain, G, is reduced to 1.0 to maintain stability as a result of the added speaker dynamics. It is seen from the dashed-dotted line representing the control-path that the uncompensated loudspeaker shifted the resonant phase from -180^o to -80^o. Rather than attenuating the first mode, mass is effectively added and the closed-loop resonant frequency shifted downward, while damping is relatively unaffected.

Next, phase adjustment is accomplished through the addition of an all-pass filter. Since $\theta_f + [\theta_s + \theta_d] = -80^0$, the required phase correction, using Equation (3.5), is $\theta_a = 280^o$.

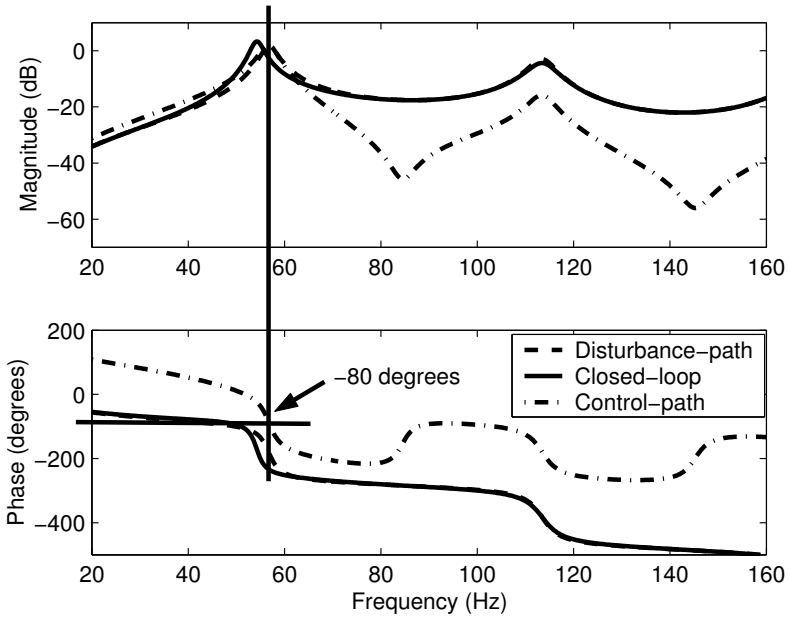

Figure 14: Predicted disturbance-path/closed-loop response with speaker dynamics.

The corresponding pole/zero location for the inverting all-pass filter from Equation (3.7) is $p = z = 425$. A stability analysis must be completed to choose the proper filter gain value. This is performed by assembling the system shown in Figure 10 with a unity gain and using the MATLAB^{TM} rlocus function. The results of the root locus analysis are seen in Figure 15.

Notice that instability will be reached at $38.1\,Hz$ with a gain of 6.61. Matching results are also obtained using the MATLAB^{TM} margin command, which computes both gain and phase margins of feedback controller. Performing a heuristic optimization, a filter gain value of $G = 1.5$ is chosen. Now, introducing the all-pass filter into the control-path results in the disturbance-path/closed-loop response shown in Figure 16, where $8\,dB$ of attenuation is now observed in the closed-loop system.

Consider now the case where control over the second mode at $\omega_c = 713\,rad/s$ $(113.5\,Hz)$ is performed. By choosing an inverting band-pass filter as the compensator, less phase correction is required of the all-pass filter. Since $\theta_f + [\theta_s + \theta_d] = 146^o$, the required phase adjustment, given by Equation (3.5) is $\theta_a = 34^o$ and Equation (3.6) yields the non-inverting

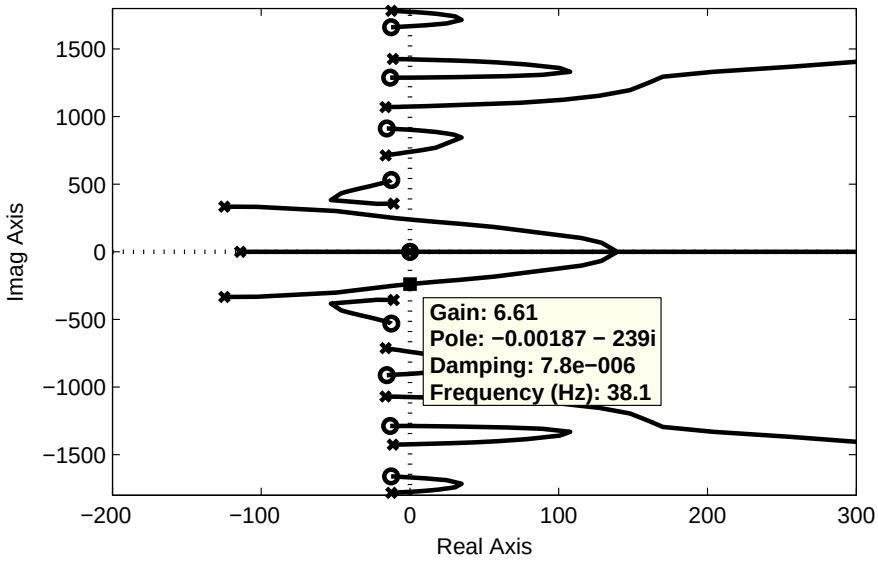

Figure 15: Root locus analysis of first mode controller

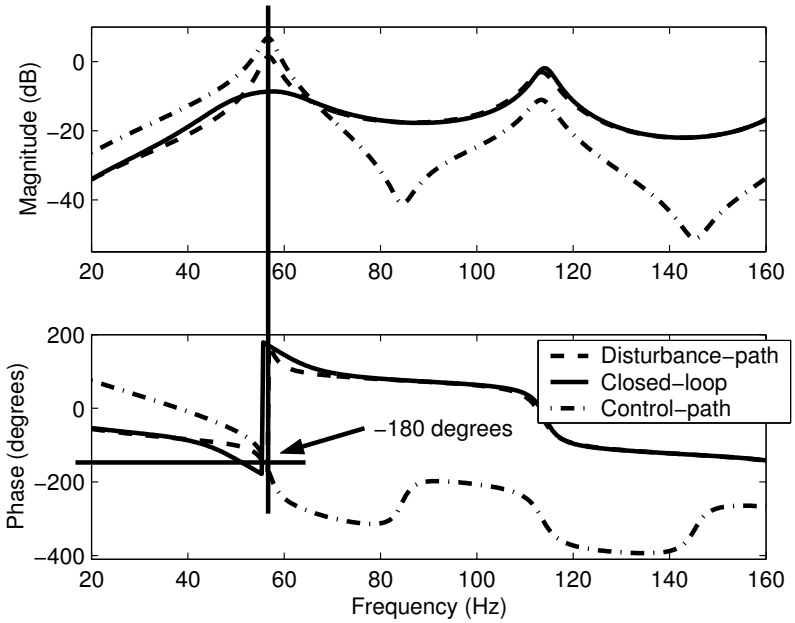

Figure 16: Predicted disturbance-path/closed-loop response using all-pass filter.

all-pass pole/zero of $p = z = 218\,\frac{rads}{s}$. Using these values and a filter damping ratio of 0.25, the resulting root locus plot for this controller is seen in Figure 17.

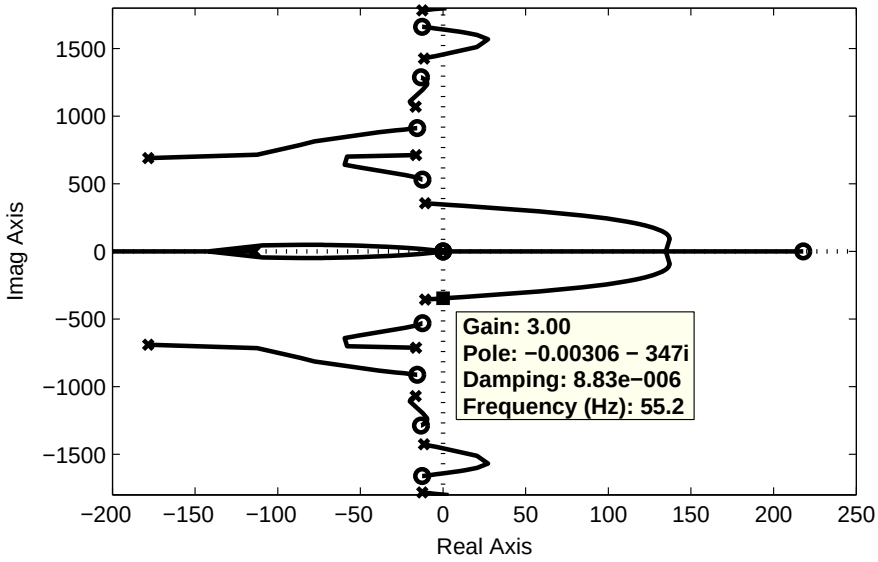

Figure 17: Root locus analysis of second mode controller

From Figure 17, it is seen that instability occurs near the first mode at a maximum allowable gain of 3.0. Again, performing a heuristic optimization, a filter gain of 0.6 is chosen, which results in disturbance-path/closed-loop magnitude response shown in Figure 18. At the second mode, it is seen that $5\,dB$ of attenuation occurs. Notice that a $3.0\,dB$ "spill-over" occurs at the first mode, which is an artifact of the loudspeaker dynamics and is not observed for structural PPF using piezo ceramics.

In the next section, the techniques developed thus far are applied to non-resonant 4^{th}-order Butterworth filters. These filters have many desirable properties that improve the overall performance of the controller.

3.3 FOURTH-ORDER COMPENSATORS

The benefit of using the band-pass filter is that it provides attenuation to the speaker dynamics in the frequency ranges above and below the control frequency, ω_c. When using the

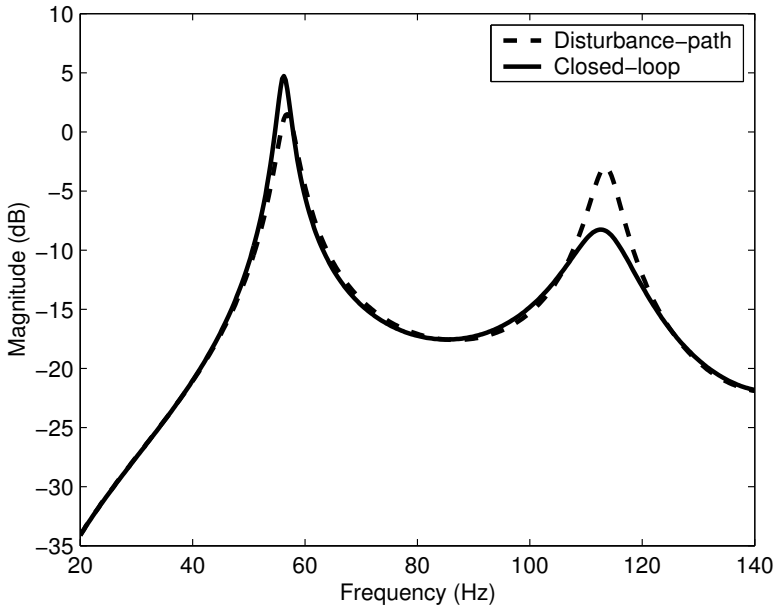

Figure 18: Predicted disturbance-path/closed-loop response for control over mode 2.

2^{nd}-order band-pass filters, this attenuation was only minimal. In this section, 4^{th}-order Butterworth filters will be used instead of the resonant filters used in the previous chapter. In addition, the designs will be limited to non-inverting filters. If an inverting filter is required, the sign is changed on the all-pass filter. It will be shown that by increasing the order of the filter from 2 to 4, the level of control can be significantly improved while causing less "spillover" into other modes. The level of complexity encountered using fourth-order Butterworth filters is only slightly greater than the second-order shown above, but the improved results justify the added complexity.

Now, consider Figure 19, which illustrates the frequency response of a 4^{th}-order Butterworth filter tuned to the second duct mode, $f_c = 113.5\,Hz$. Note, a filter bandwidth of $35\,Hz$ was chosen, which is similar to the bandwidth of the first few duct modes.

From Figure 19, it is seen that that the magnitude response of the Butterworth filter provides close to $50\,dB/dec$ of attenuation on both sides of the center frequency, f_c. This attenuation rate is much larger than the $20\,dB/dec$ provided by the resonant band-pass filter shown in Figure 12(b). In addition, differences are also seen in the phase response. At low frequency regions, the Butterworth has a phase response close to 180^o, as opposed to the

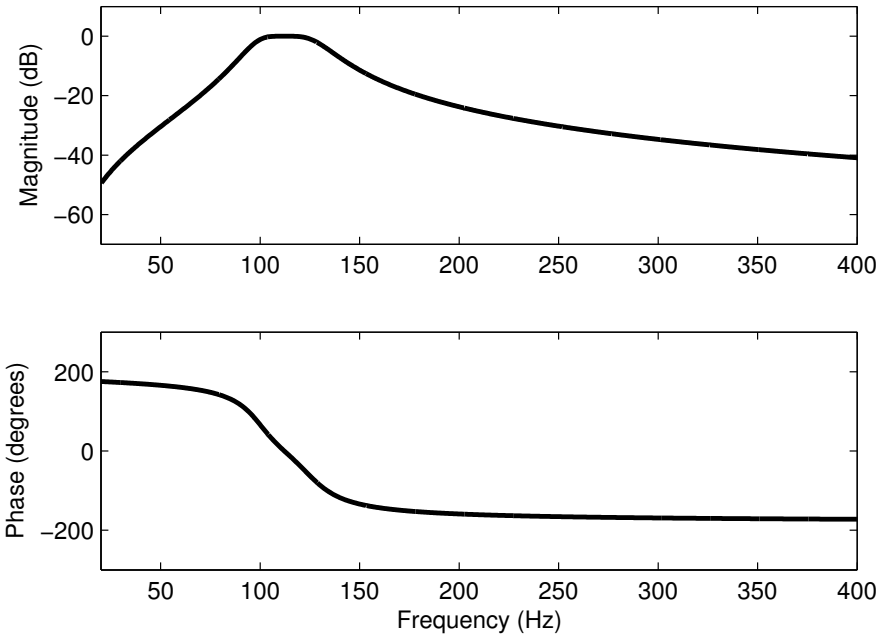

Figure 19: Butterworth response tuned to second duct mode.

90^o reported by the resonant BPF. On the other hand, at high frequencies, the Butterworth filter approaches -180^o. This is an addition of -90^o, when compared to the resonant BPF. At the center frequency, however, both the resonant and Butterworth filter have a phase response of 0^o.

The next task is to develop a controller that makes use of both a collocated sensor/actuator pair and the filter shown in Figure 19. To begin, consider Figure 20, where the filter response shown in Figure 19 is combined with the duct control-path and loudspeaker. At this point, no phase compensation has been added to the control-path.

It is seen from the magnitude response shown in Figure 20 that this control-path provides the desired attenuation in regions above and below the control frequency, f_c. As a result, this control-path will more effectively target the duct mode of choice when compared to control-paths such as the one shown in Figure 16. Like previous examples, the control-path needs phase correction. Using Equation (3.1), θ_c is seen to be -32.1^o, thus, from Equation (3.5), the supplemental angle, θ_a, is 212.1^o. From Equation (3.7), the inverting all-pass filter pole is calculated to be $p = z = 205.7\,\frac{rads}{s}$. Now, the filter network is added to the control

path and a root-locus analysis is performed. The results of this simulation can be found in Figure 21.

From Figure 21, it is seen that the closed-loop poles will enter the right-hand plane at a frequency of 171.0 Hz when the filter gain, G is greater than 13.4. This is a 447% increase in useable gain over the results predicted in Figure 17 for the resonant band-pass filter tuned to the second duct mode. When the gain becomes large, an observable mode is noticed in the stable closed-loop response. To prevent this, a filter gain value of 1.25 is chosen, which results in closed-loop response shown in Figure 22.

The closed-loop system predicted in Figure 22 shows that about 5.5 dB of attenuation has been achieved. Also, the "spillover" seen in the first mode (Figure 18) has been nearly eliminated. The remaining modes are left nearly untouched, with no more than $\pm 0.2\,dB$ differences between the disturbance-path and the closed-loop system.

3.4 CONTROL WITH NON-COLLOCATED SENSOR/ACTUATOR PAIR

Up to this point, the controllers presented have all utilized collocated sensor/actuator pairs, which was consistent with other works in PPF [17, 26, 25]. It is now shown that the phase compensation all-pass filter has the added benefit of allowing the designer to adjust the phase of both minimum and non-minimum phase systems. As a result, the use of both collocated and non-collocated sensor/actuator pairings are permitted. This case will be presented without the detailed step by step process and stability analysis. Before beginning, however, it is important to briefly discuss how to properly locate the sensor for the system shown in Figure 4. If the sensor is improperly located, the closed-loop system will not produced the desired results. To illustrate this, examine Figure 23 where the first three mode shapes, described by Equation 2.3, are shown.

It is seen from Figure 23 that if the first mode, $n = 1$, is to be controlled, placing the sensor at the midpoint of the duct would result in zero control. Likewise, for control of the third mode, $n = 3$, placing the sensor 0.5 m from the end would also result in zero control. However, if the sensor is situated such that it is collocated with either the disturbance source or the control source (corresponding to end points in Figure 23, then all of the modes are

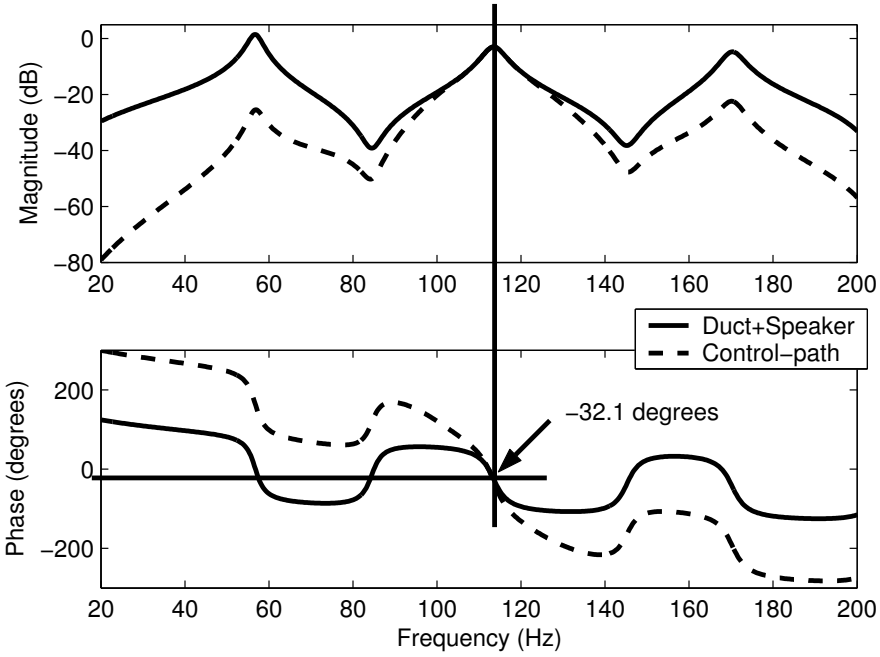

Figure 20: Predicted control-path response.

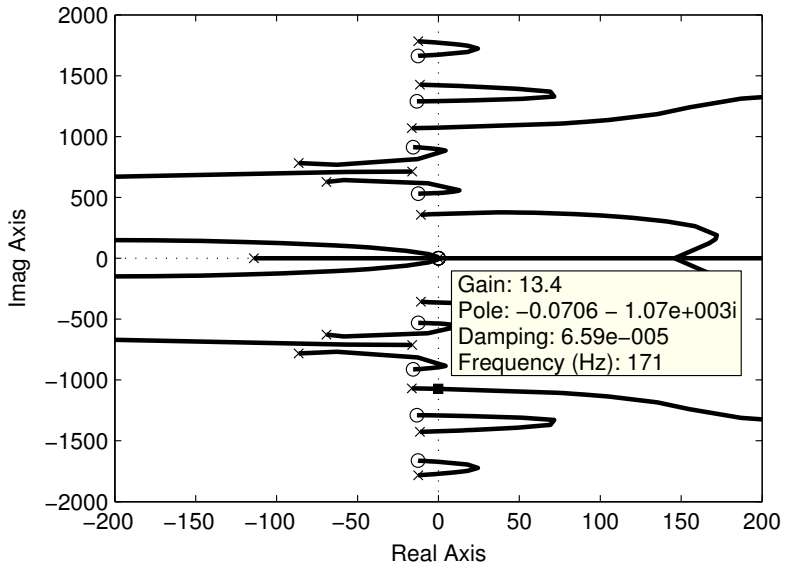

Figure 21: Root-locus of control-path with Butterworth filter.

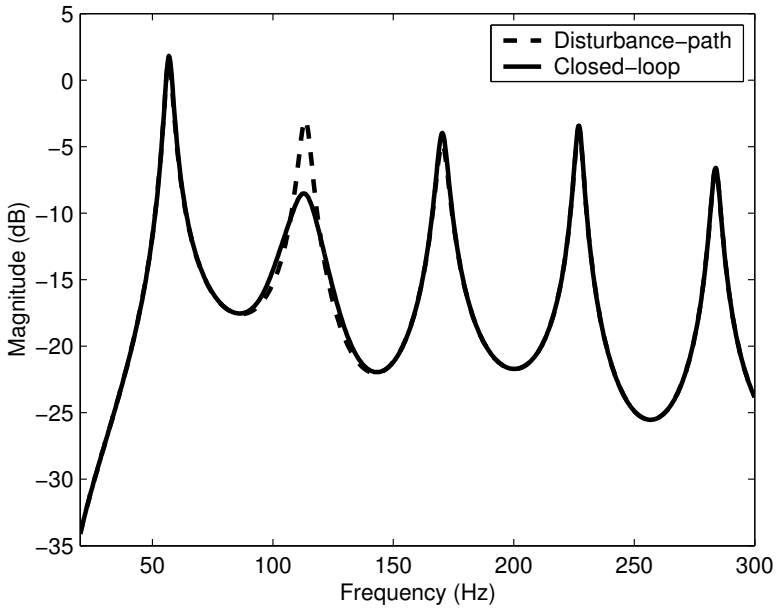

Figure 22: Predicted closed-loop response with control over mode 2.

observable by the sensor. With that, now consider the response of duct control-path and loudspeaker when the control sensor is placed beneath the disturbance loudspeaker. In other words, $x_{sen} = x_1$. The results of this are seen in Figure 24.

Notice that the phase response is no longer non-minimum. Since additional phase is introduced by the all-pass filter, the non-minimum behavior of this control-path can be compensated. With this configuration, a controller that targets the first duct mode, $f_c = 56.6\,Hz$, is now presented. Note that band-pass filters are required for non-collocated sensor/actuator pairs since the non-minimum phase characteristics will destabilize low frequency modes if a low-pass filter is used. From Figure 24, the phase of the duct control-path and loudspeaker is seen to be -178^o. This is a case where the phase response is within 2% of -180^o, therefore, the filter network will contain a Butterworth band-pass filter, but no all-pass filter. The results of the disturbance-path/closed-loop response with a filter gain of $G = 2.5$, a bandwidth of $35\,Hz$, and $x_e = x_2$ are seen in Figure 25.

For this scenario, it is seen that $9.5\,dB$ of reduction is exists in the first mode. A slight amount of control is also noticed in the second mode. The non-minimum characteristics are of use if "spillover" exists in a mode that is adjacent to the targeted mode. By switching the

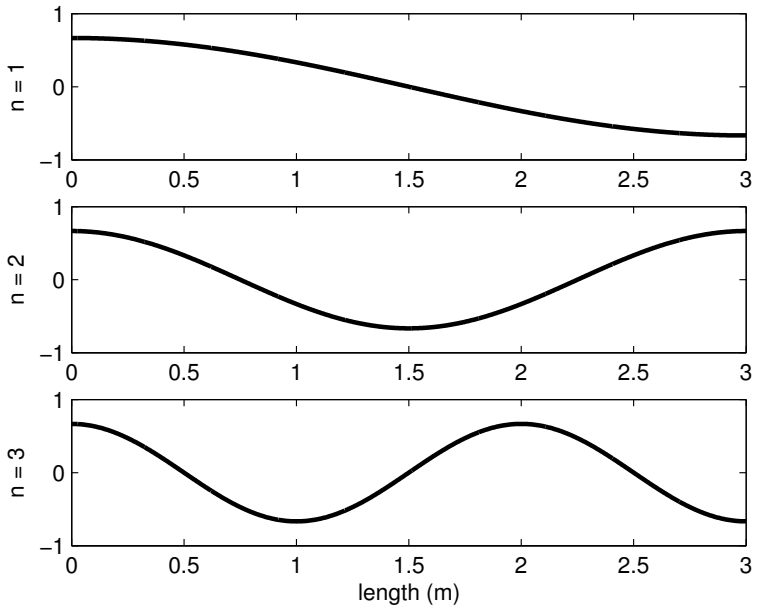

Figure 23: Illustration of sensor placement using duct mode shapes

sensor location to be collocated with the disturbance source, the "spillover" in the adjacent mode should be reduced.

Listed in Appendix C is a MATLAB^{TM} program that is used to design an appropriate phase-compensated filter network for an acoustic system. This code can be used to design both resonant and Butterworth filter networks for both collocated or non-collocated sensor/actuator pairings. Although it has been written to make use of the duct and loudspeaker models in Appendices A and B, it can easily be modified to work with several acoustic systems.

3.5 MULTIMODAL CONTROL

The final topic covered in this chapter is multimodal control, in which two or more 4^{th}-order Butterworth filter networks are developed, each of which is tuned to a separate duct mode frequency. Each of the filter networks is developed separately, using the techniques outlined thus far. These filter networks are then connected in parallel so that voltage outputs are all

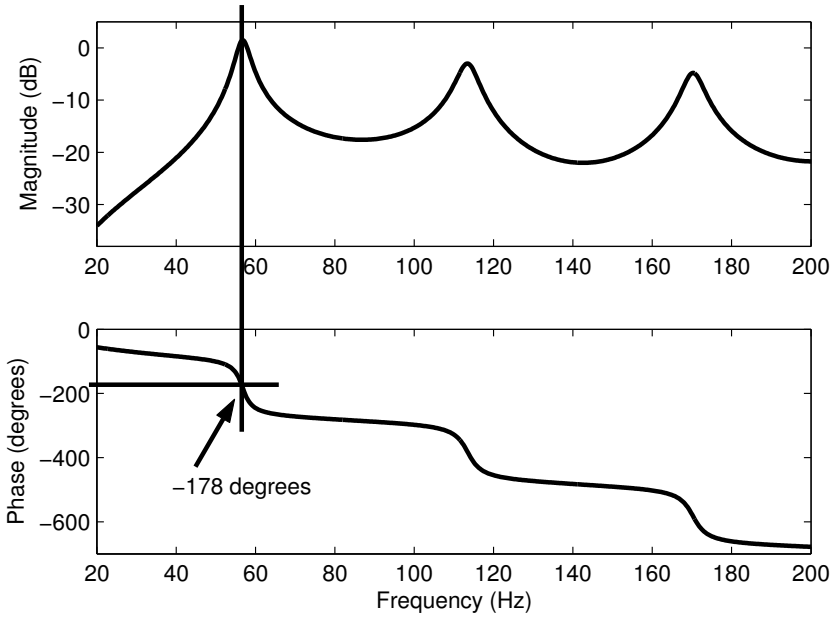

Figure 24: Predicted results of duct+loudspeaker when $x_{sen} = x_1$.

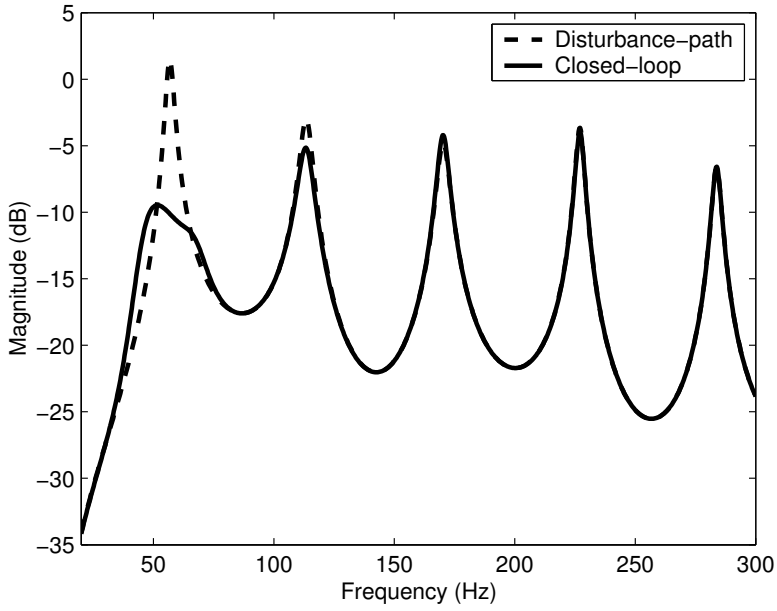

Figure 25: Predicted disturbance-path/closed-loop results when $x_{sen} = x_1$, $x_e = x_2$.

fed to the control loudspeaker. A sample block diagram of a dual mode controller is seen in Figure 26.

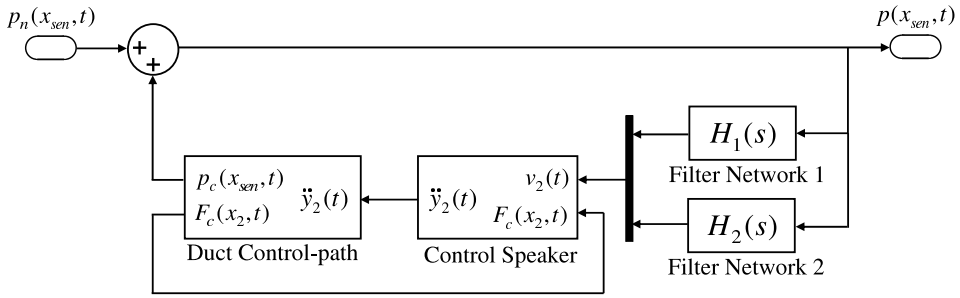

Figure 26: Schematic of multimodal controller.

In order for multimodal control to be effective, it is required that the modal spacing of the plant be sufficiently large [17, 18]. If this is not the case, the filter network will not provide enough attenuation to the plant and loudspeaker dynamics between the modes, thus causing large reductions in the stability range of the closed-loop case. Regardless of the modal spacing, the overall performance at a single mode will be affected when additional filter networks are added to the system. This effect is more pronounced when targeted modes are adjacent to each other. To test this, a dual mode controller, such as that shown in Figure 26, will be designed to target the first and second duct modes, $f_1 = 56.6\,Hz$ and $f_2 = 113.5\,Hz$ respectively.

For this configuration, a filter network tuned to the first duct mode is designed and combined in parallel with a filter network identical to that shown in Figure 20 and tuned to the second duct mode. The Butterworth filters each have a bandwidth of $35\,Hz$. Both filter networks are found to require inverting all-pass filters to provide the required 180^o at each of the targeted modes. Listed in Table 2 are the parameters obtained from the design algorithm for each filter network, along with the heuristically chosen gain values, which are within the stability range provided by the MATLAB^{TM} rlocus function.

Using the values listed in Table 2, the control-path frequency response is obtained. The results of this simulation are shown in Figure 27. It is seen that the phase response at both f_1 and f_2 are indeed a multiple of 180^o. The magnitude response also provides the required

Table 2: Dual mode controller design parameters.

Mode 1 Filter Network		*Mode 1 Filter Network*	
Param.	Value	Param.	Value
f_c	$56.6\,Hz$	f_c	$113.5\,Hz$
θ_c	-11.8^o	θ_c	-32.2^o
θ_a	191.7^o	θ_a	212.2^o
p, z	$36.5\,\frac{rads}{s}$	p, z	$205.7\,\frac{rads}{s}$
G	1.5	G	1.25

attenuation in those modes beyond the second duct mode. Note that when both filter gains are equal to 1.0, instability occurs at $264\,Hz$ when the overall control-path gain exceeds 8.35. As previously stated, this is seen to be 37.7% lower than the single controlled mode shown in Figure 21.

Finally, the closed-loop response is determined. The results of this simulation are seen in Figure 28. Notice that $9.5\,dB$ of attenuation is seen in the first mode at $56.6\,Hz$ and $5.5\,dB$ of reduction at $113.5\,Hz$. Also, notice the $1.0\,dB$ of "spillover" that occurs at $170.3\,Hz$. This is slightly larger than that reported in Figure 22 and is a result of the added dynamics of having multiple filter networks present in the controller.

Thus far, several controllers have been designed and simulated. The next step is to verify the simulated controllers against experimental examples. In the next chapter, two experimental controllers are developed and applied to an experimental test bed. The first controller is an example that makes use of a resonant band-pass filter, and the second is a multimodal case in which Butterworth filters are used.

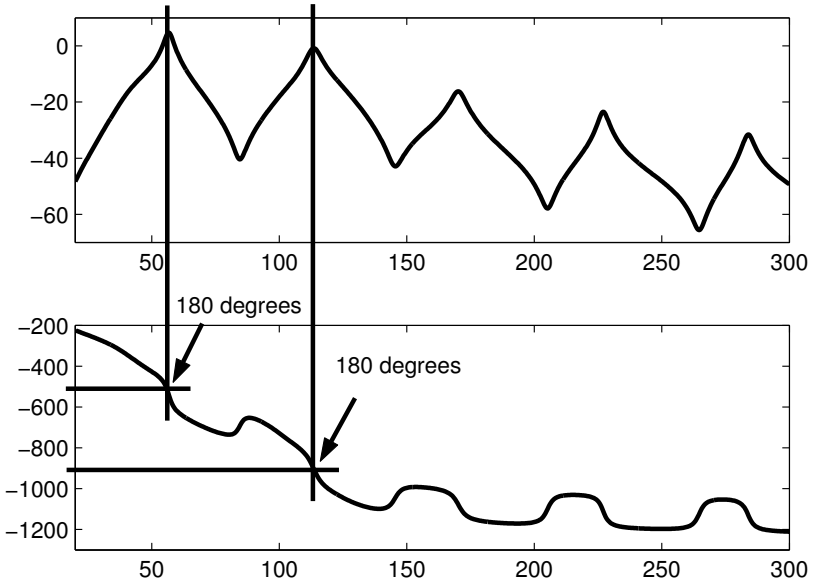

Figure 27: Predicted control-path response tuned to modes 1 and 2.

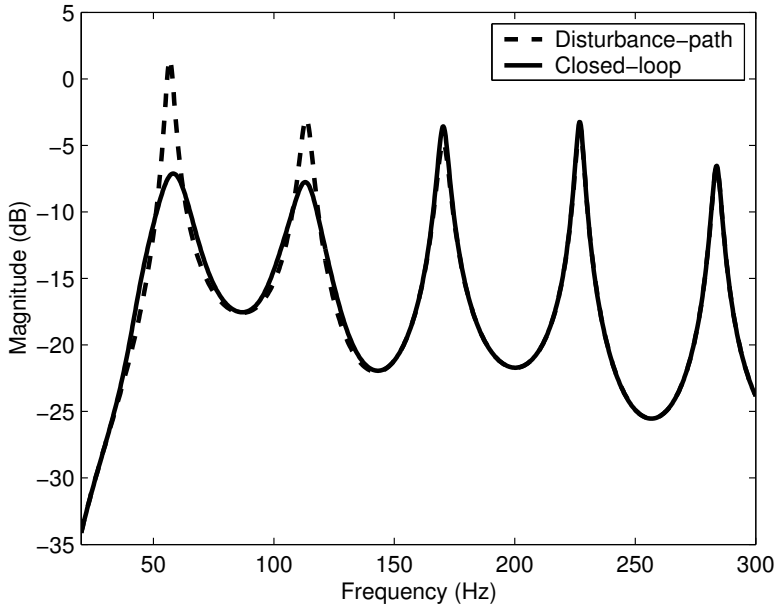

Figure 28: Predicted disturbance-path/closed-loop response for control over modes 1 and 2.

4.0 EXPERIMENTAL DEMONSTRATIONS

4.1 DESIGN AND RESPONSE OF SECOND-ORDER CONTROLLER

In order to verify the ANC method discussed in this paper, an ANA compensator was designed to control the first acoustic mode of the experimental test bed shown in Figure 29. The duct is constructed of $1.9\,cm$ thick hard plywood and is sealed with silicone caulking. The internal dimensions are consistent with the simulated model and are provided in Table 1. Both the disturbance and control loudspeakers (Peerless 832592) are mounted in identical sealed boxes having an internal volume of $2,304\,cm^3$. Ten equidistant, sealable ports are located along the top edge of the duct for error measurement purposes, and another port is collocated with the center of the control loudspeaker to provide the input signal to the controller. Model Mike-28 microphones by All Electrocics Corp were used for pressure measurements.

The measured frequency response for the uncontrolled plant was presented in Figure 7. The input to the disturbance loudspeaker was a white noise signal with a bandwidth of $1000\,Hz$, and the output was a pressure measurement at x_2. All data for the experiments were collected using a SigLab MC-2084 signal analyzer.

4.1.1 Compensator Design

For the experiment, an inverting band-pass filter was found to provide the optimum gross phase adjustment for the first frequency mode, $f_c = f_1$. By examining the experimental open-loop data from Figure 7, f_1 was found to be $54.8\,Hz$, which is 3.28% lower than the predicted value used in the simulation. In order to realize the 2^{nd}-order band-pass filter, a Burr-Brown

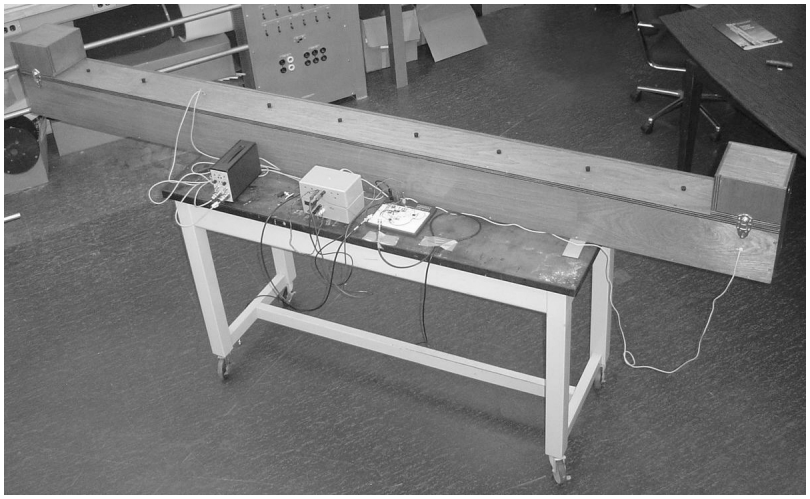

Figure 29: Experimental test bed.

UAF42AP universal filter circuit was used, where the parameters were determined using the BB Filter42 design tool [24]. The resulting resistance values and quality number for the band-pass filter, which cooresponds to the PP3 subcircuit in Reference [24], are included in Table 3 below.

Each of the resistors provided by the design program were trimmed as necessary, using potentiometers until f_c was within 2% of f_1. With the filter added to the control-path, it was found that $\theta_c = 100^o$, thus, an inverting all-pass filter was selected with a phase adjustment (Equation (3.5)) of $\theta_a = -80^o$. From Equation (3.7), the required all-pass filter pole/zero was set at $p = z = 341\,\frac{rads}{s}$ and the inverting behavior was realized by adding a unity gain inverting op-amp circuit (Figure 30(b)) in series with a non-inverting all-pass filter [23] (Figure 30(a)).

Note that v_{sen} from Figure 30 is the voltage output from the control sensor microphone. For the all-pass filter in Figure 30(a), the electrical components were chosen from the pole/zero location using

$$p = z = \frac{1}{R_a C_a}. \tag{4.1}$$

The values of R_a, C_a, and the value of R_g used in the inverting op-amp circuit are also found in Table 3. Notice that a variable feedback resistor is shown in Figure 30(b) and was

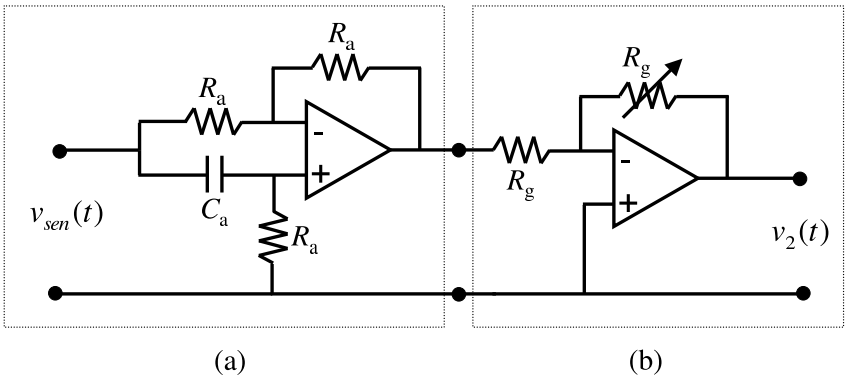

Figure 30: Schematic for inverting all-pass filter network.

used to provide adjustment to the overall gain of the control-path. With this, the frequency response of the fully-compensated control-path, where $\theta_c(\omega_c) = 180^o$, is shown in Figure 31. It is observed that precisely 180^o of phase shift occurs at the targeted mode.

Table 3: Compensator parameters.

Band-pass filter		*All-pass filter*	
Param.	Value	Param.	Value
$R_{F1,2}$	$2.95\,M\Omega$	R_a	$744\,\Omega$
R_Q	$6.98\,k\Omega$	C_a	$3.3\,\mu F$
R_G	$50.0\,k\Omega$	R_g	$1.0\,k\Omega$
Q	2.72	-	-

4.1.2 Closed-loop Response

The closed-loop response for an error position of $x_e = 2.90\,m$ was obtained using the controller developed above. The control-path gain, G, which was varied, using the feedback resistor from Figure 30, was heuristically optimized from zero to the maximum where instability occurred. A close-up view of the first frequency mode can be seen below in Figure 32. The closed-loop response shown by the solid line ($G1$) represents a moderate amount

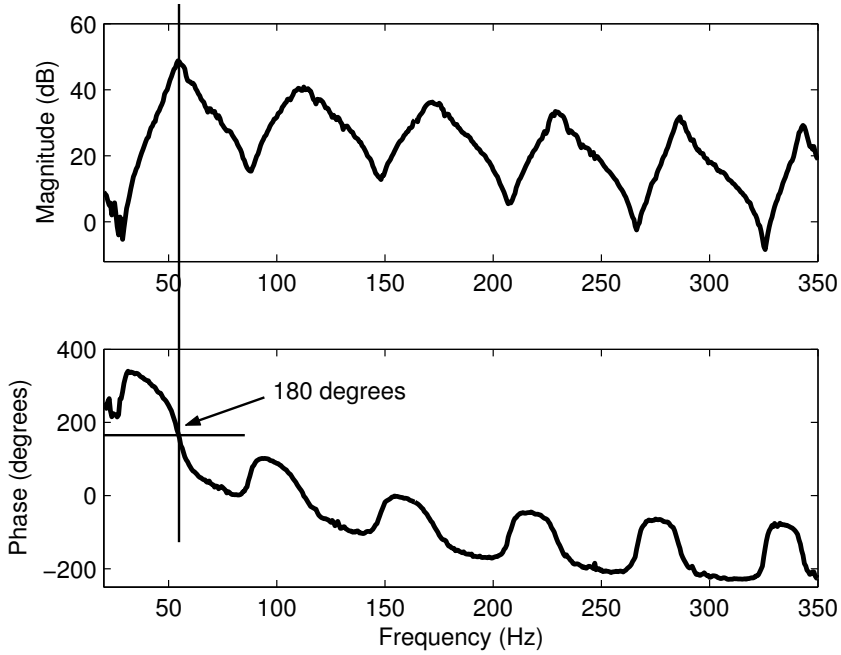

Figure 31: Measured fully compensated control-path.

of control gain with about $6\,dB$ reduction observed, while the dashed-dotted line ($G3$) is near instability and exhibits about $13\,dB$ of control in the first mode. Choosing an intermediate gain ($G2$), the closed-loop response between the disturbance loudspeaker and error microphone over a $500\,Hz$ frequency range is plotted in Figure 33.

A small amount of spillover is noted in the second mode at $113\,Hz$. This result is consistent with the phase response given by Figure 31, which shows approximately 0^o of phase at the second mode frequency. Higher frequency modes at 170, 227, 283, and $340\,Hz$ have more than 90^o of phase shift and hence, a small degree of control is noted in Figure 33 for these modes. Using a 4^{th}-order filter minimizes the influence on untargeted modes.

4.2 DESIGN AND RESPONSE OF MULTIMODAL CONTROLLER

The final experiment performed illustrates an ANA multimodal controller utilizing two 4^{th}-order Butterworth filters with a collocated sensor/actuator pair. For this demonstration, both the fundamental and the second duct modes were chosen as the targeted regions of

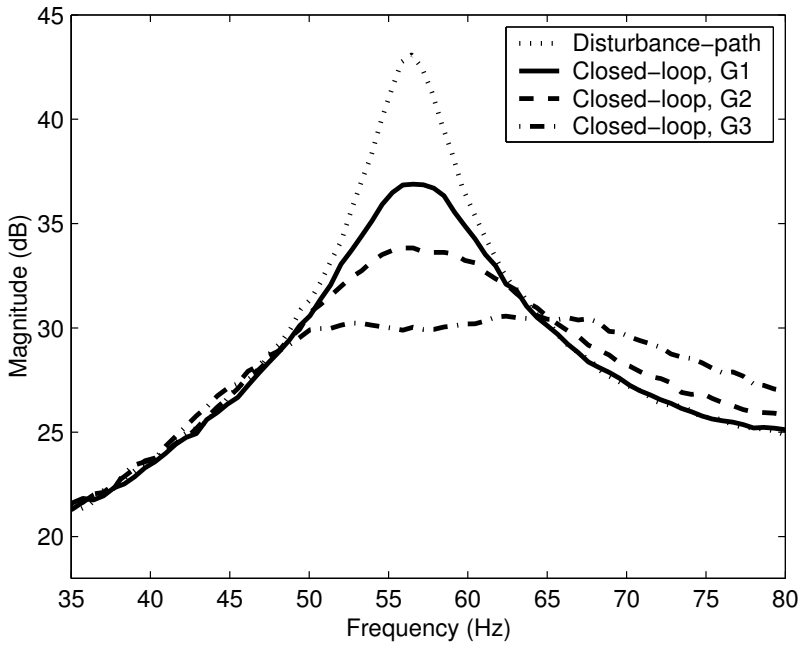

Figure 32: Measured disturbance-path/closed-loop response for various gain values.

control. The Butterworth filters, as before, were constructed using Burr-Brown UAF42AP universal filter circuits in conjunction with the BB Filter42 design tool [24]. Each of the filters was designed and tested individually before being combined to form the total controller.

To control the fundamental duct mode, a 4^{th}-order Butterworth filter was designed using a series connection of two PP1 subcircuits, as dictated by the BB filter design tool, such that the center frequency was tuned to $f_c = 54.8\,Hz$. The subcircuit component values, given in Table 4, were each trimmed to within 2% of their reported value. Adding this filter to the control-path yielded a phase response, θ_c of 50^o. Thus a non-inverting all-pass filter (schematic shown in Figure 30(a)) with a phase response of $\theta_a = 130^o$ at f_c was required to properly adjust to phase to 180^o. This corresponds to an all-pass pole/zero location of $p = z = 741\,\frac{rads}{s}$. Using Equation (4.1), the all-pass parameters, C_a and R_a, were calculated to be $6.75\,\mu F$ and $200\,\Omega$ respectively. For this configuration, a non-inverting pure gain circuit was also needed to allow gain adjustment to the control-path. This was accomplished by switching the polarity on the control-speaker and using the inverting gain circuit shown in Figure 30(b). As before, R_g was selected to be $1.0\,k\Omega$.

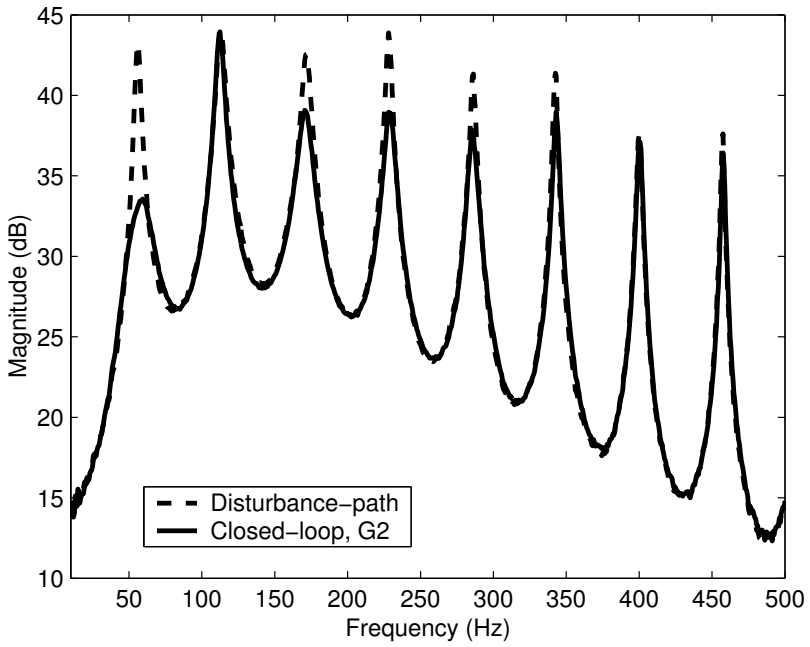

Figure 33: Measured Disturbance-path/closed-loop response over 500 Hz frequency range.

Using the same procedure, a second filter-network tuned to the second duct mode, $f_c = 113\,Hz$, was developed. Again, two series connected PP1 subcircuits were required to construct the Butterworth filter. The corresponding component values for each subcircuit are also listed in Table 4. Again, by adding this filter to the control-path, it was found that the phase response, θ_a was 178^o. Since this is only 1.1% from the required 180^o, no all-pass filter was needed. In order to adjust the overall gain of this filter network, a non-inverting pure gain circuit was required, however, since the control-speaker polarity was reversed for the mode 1 controller, a second inverting op-amp circuit was used with R_g set to $1.0\,k\Omega$.

Before measuring the overall frequency response of the control-path, the two controllers developed above were hooked up in parallel as shown in Figure 26. Thus, the combined filter network received a pressure reading from the control sensor as an input, while a single voltage was fed into the control loudspeaker. With this setup, the control-path was measured to verify that it produced the proper magnitude and phase response. The results of this measurement are seen in Figure 34.

Table 4: Multimodal Butterworth filter compensator parameters.

Band-pass filter 1				*Band-pass filter 2*			
Subcircuit 1		Subcircuit 2		Subcircuit 1		Subcircuit 2	
Param.	Value	Param.	Value	Param.	Value	Param.	Value
$R_{F1,2}$	$2.26\,M\Omega$	$R_{F1,2}$	$3.57\,M\Omega$	$R_{F1,2}$	$1.27\,M\Omega$	$R_{F1,2}$	$1.58\,M\Omega$
R_Q	$18.7\,k\Omega$	R_Q	$18.7\,k\Omega$	R_Q	$6.98\,k\Omega$	R_Q	$6.98\,k\Omega$

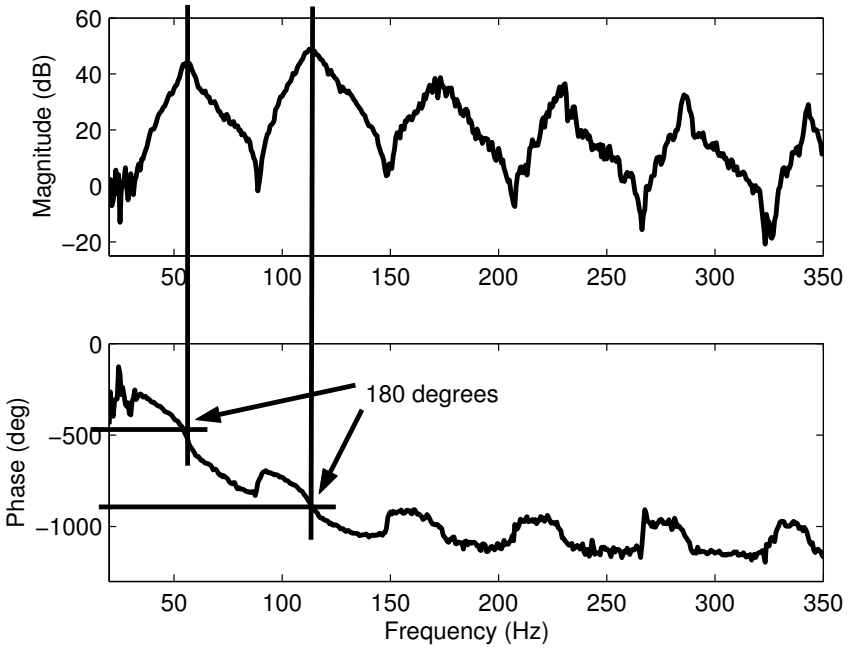

Figure 34: Measured fully compensated multimodal control-path.

Notice that at both $54.8\,Hz$ and $113.0\,Hz$, a phase angle of 180^o has been achieved, as indicated by the markers. This filter network was then added to the plant. The measured results of the closed loop for three different gain settings are shown in Figure 35. Since control exists in both the fundamental and second duct mode, it was found that stability range for this controller was greater than that of the single mode controller (Figure 33) where instability occurred at the second mode.

Each gain value reported in Figure 35 represents the combined gains on each of the two filter networks. The solid line ($G1$) represents a small amount of gain; the dashed line ($G2$) represents a modest amount of gain; and finally, the dash dot line ($G3$) corresponds to a heuristic optimization of the two gain values. Using this value, the frequency response over a $500\,Hz$ range was measured and can be seen in Figure 36.

For this gain configuration, a $10.0\,dB$ reduction is seen in the first duct mode and about $8.0\,dB$ is reported in the second. Note that additional control is also reported in the third mode and, to a lesser degree, in the fourth mode. As with the 2^{nd}-order compensation filter, this is a result of the control-path having a phase shift of more than 90^o and adequate gain at each of the resonances.

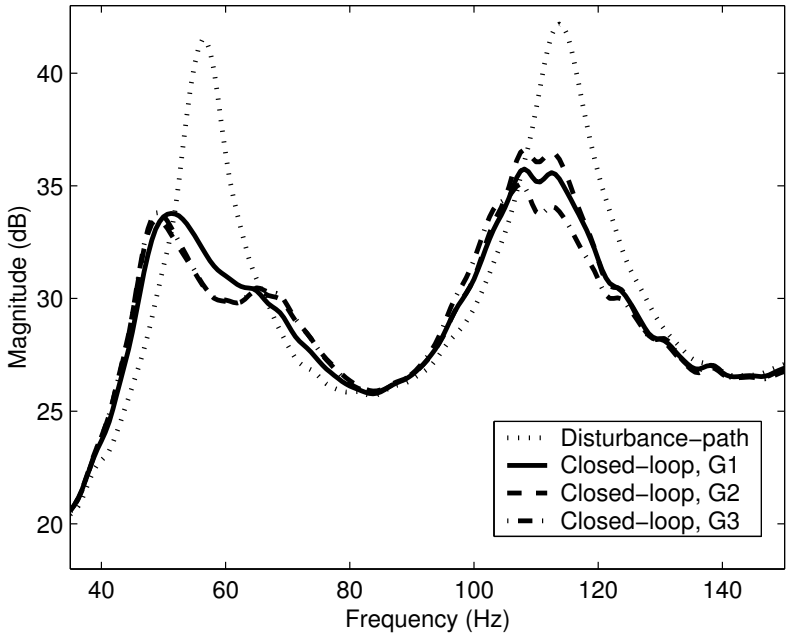

Figure 35: Measured disturbance-path/closed-loop response for various gain combinations.

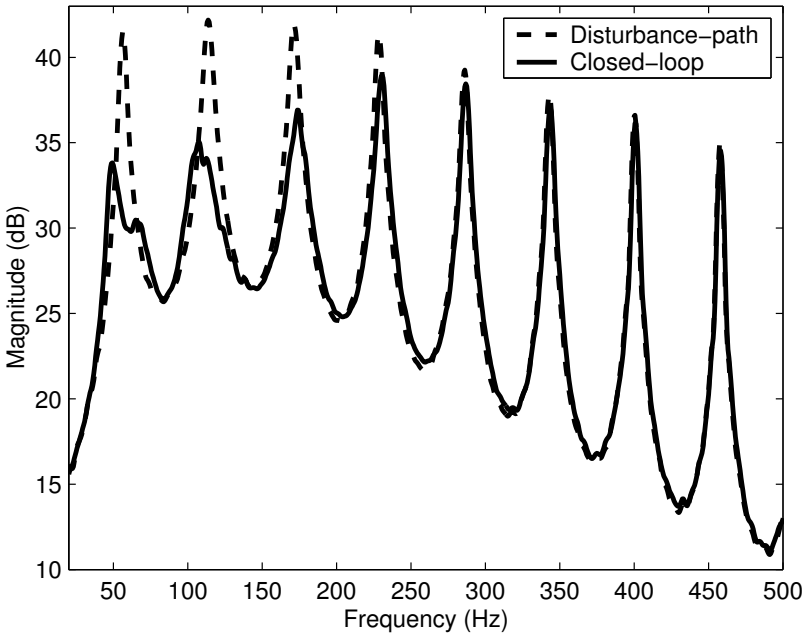

Figure 36: Measured disturbance-path/closed-loop response for gain value $G3$.

5.0 CONCLUDING REMARKS

A new technique has been developed for controlling single or multiple modes in acoustic enclosures. This device is referred to as an active noise absorber (ANA). Similar to positive position feedback (PPF) for structures, an ANA control compensator can make use of damped, resonant filters as control compensators. However, it is shown that improved performace is obtained by using 4^{th}-order Butterworth filters. Unlike structural cases in PPF, where the piezo crystal actuators are virtually dynamicless in the low frequency region, acoustic actuators (loudspeakers) add dynamics to the closed-loop system. The phase response of the added dynamics degrade both the performace and stability of the control system and must be compensated. Phase compensation for an ANA is achieved by combining an all-pass filter with the control filter so that the control-path provides $\pm 180^o$ of phase at the desired control frequency. A method of gross phase compensation (within $\pm 90^o$ of target) is achieved by choosing either a BPF or LPF filter, which may be combined with an inverting circuit. Low-pass filters are found to work well for the fundamental duct mode, while band-pass filters are found to work for higher frequency modes where the phase response of the loudspeaker is more pronounced.

The phase-compensation abilities of the all-pass filter are found to have a second benefit. Unlike previous examples in PPF, an ANA controller does not require collocated sensor/actuator pairs. The phase-shaping characteristics of the all-pass filter allow for the compensation of non-minimum phase response that results when non-collocated sensor/actuator pairings are used.

To illustrate the design and response of the ANA controller, a duct model that has a control speaker at one end and a disturbance speaker at the other was created. Simulated results demonstrate individual control of the first two modes using 2^{nd}-order compensators,

while multimodal control of the first and second modes is achieved using a 4^{th}-order Butterworth network. One experimental demonstrations targeted the first duct mode using a 2^{nd}-order BPF. The gains were heuristically chosen to provide a $10\,dB$ reduction. Some control in adjacent modes was also observed. Spillover was minimal, presumably due to the roll-off of the band-pass filter in the control compensator. A second experimental demonstration provided simultaneous control of the first two duct modes using a pair of 4^{th}-order Butterworth band-pass filters. The roll-off provided by the 4^{th}-order filter helped minimize effects of the controller on non-targeted modes.

APPENDIX A

MATLAB™ CODE FOR DUCT

```
function sys=ductFreq(xLoc,X,Ly,xSen)

%%% Duct properties %%%

Lg = 10*12*.0254; % m, duct length
c = 346; % m/s, sound speed
rho = 1.225; % kg/m^3, density
zeta = 0.008; % duct damping ratio

N  = 20;     % number of pressure modes...
n = 1:N;
Wn = pi*c/Lg*(1:1:N);     % vector of duct natural frequencies
bnP = (4*rho*c^2*Ly)/(Lg*pi)*(sin(Wn/c*X.X12)-sin(Wn/c*X.X11))./n;
dnP = (2*Ly)/pi*(sin(Wn/c*X.X12)-sin(Wn/c*X.X11))./n;
bn = (4*rho*c^2*Ly)/(Lg*pi)*(sin(Wn/c*X.X22)-sin(Wn/c*X.X21))./n;
dn = (2*Ly)/pi*(sin(Wn/c*X.X22)-sin(Wn/c*X.X21))./n;

n = 1:N;
numRows = (N*2);
```

```
% create A matrix and ones along I,J diaganal
AA = zeros(numRows);
for I = 2:2:numRows
    AA(I-1,I) = 1;
end

zeta = [linspace(0.03,0.008,4) 0.007*ones(1,size(Wn,2)-4)];
%zeta = linspace(0.005,0.0001,size(Wn,2));

for I = 1:2:numRows-1
%    ductDamp = 2*zeta*Wn((I+1)/2);
    ductDamp = 2*zeta((I+1)/2)*Wn((I+1)/2);
    Wn_sq = Wn((I+1)/2)^2;
    AA(I+1,I) = -Wn_sq;
    AA(I+1,I+1) = -ductDamp;
end

BB = zeros(numRows,2);

for I = 1:2:numRows-1
    BB(I+1,1) = bnP((I+1)/2);
    BB(I+1,2) = bn((I+1)/2);
end

DD  = zeros(4,2);

bs    = (2/Lg)*cos(n*pi*xLoc/Lg);
bsSen = (2/Lg)*cos(n*pi*xSen/Lg);

CC = zeros(3,numRows);
```

```
for I=1:2:numRows-1
    % X.X11, X.X12, Pressure output to the noise Speaker
    CC(1,I) = dnP((I+1)/2);
    % xLoc, Error signal at a point
    CC(2,I) = bs((I+1)/2);
    % xSens, Pressure output to the sensor
    CC(3,I) = bsSen((I+1)/2);
    % X.X21, X.X22, Pressure output to the control Speaker
    CC(4,I) = dn((I+1)/2);
end

sys = ss(AA,BB,CC,DD);
```

APPENDIX B

MATLAB^{TM} CODE FOR LOUDSPEAKERS

```
function sys = noiseSpeak

% Box parameters
L = 20/100-6/100;
W = L;
H = 15/100-6/100;
Vb = L*W*H;                % box volume

% physical parameters
rho = 1.225;       % kg/m^3, density
c = 346;   % m/s, sound speed

% speaker parameters
Ms=9.2/1000;               % mass of speaker cone (kg)
Bl=6.7;                    % Bl constant (N/A)
Rs=8;                      % system resistance (Ohms)
Ls=.9/1000;                % total system inductance (Henreys)
Km = (1/0.85)*1000;        % speaker spring constant (N/m)
Bm = 1.74;                 % damping constant (N*s/m)
Sk = pi*(10.4/100)^2/4;    % speaker area (m^2)
```

```
Kb = (pi*Sk^2)^2*(rho*c*c)/Vb;
Ks = Km + Kb;

Vas = 8.7*.001;          % volume eq
alpha = Vas/Vb;
Qtc = sqrt(alpha + 1)*.34;

Wn = sqrt(Ks/Ms);
Bb = Ms*Wn/Qtc;
Bs = Bm+Bb;

ASpN = [0 1 0 0;
        0 -Rs/Ls 0 -Bl/Ls;
        0 0 0 1;
        0 Bl/Ms -Ks/Ms -Bs/Ms];

%BSpN = [0 0;1/Ls 0;0 0;0 -Sk/Ms];   % input matrix
BSpN = [0 0;1/Ls 0;0 0;0 -1/Ms];     % input matrix (voltage, pressure)
CSpN = [0 Bl/Ms -Ks/Ms -Bs/Ms];      % output matrix (acceleration observer)
%DSpN = [0 -Sk/Ms];                  % feedthrough matrix
DSpN = [0 -1/Ms];                    % feedthrough matrix

sys = ss(ASpN,BSpN,CSpN,DSpN);
```

APPENDIX C

MATLAB™ CODE UTILIZING DESIGN PROCEDURE

```
%%%%%%%%%%%%%%%%%%%%%%%%%%%%%%%%%%%%%%%%%%%%%%%%%%%%%%%%%%%%%%%%%%%%%%%%
% M file that generates the appropriate control filter and %
% all-pass filter for duct system                          %
%%%%%%%%%%%%%%%%%%%%%%%%%%%%%%%%%%%%%%%%%%%%%%%%%%%%%%%%%%%%%%%%%%%%%%%%

close all; clear all;

x1 = 4*.0254;                          % m, location of speaker 1 (noise)
x2 = 116*.0254;                        % m, location of speaker 2 (control)
X = struct('X11', x1-0.0461, 'X12', x1+0.0461, ...
     'X21', x2-0.0461, 'X22', x2+0.0461);
Ly = .0922;

%% get sensor and error locations
senLoc = input('Enter the location of the sensor as a multiple of x2 (eg x2/3): ');
errLoc = input('Enter point of measure as a multiple of x2: ');

%% get sysetm models
sysD = ductFreq(errLoc,X,Ly,senLoc);
sysC = noiseSpeak;
```

```
sysN = noiseSpeak;

%% create openloop system.
sysTemp = append(1,sysN,sysD);
Q = [2 1;3 3;4 2];
sysOL = connect(sysTemp,Q,1,4);

%% get control frequency
Wns = unique(sort(abs(pole(sysD))));
index = input('Enter mode number to control: ');
ctrFreq = Wns(index);
disp(['      Control Frequency: ' num2str(ctrFreq/2/pi) ' Hz']);
disp(' ');

%% get phase of plant and control speaker
Q = [2 5;4 4];
sysCD = connect(append(sysD,sysC),Q,3,3);
[Mcd,PHcd] = bode(sysCD,ctrFreq);

%% create filter
order = input('Enter an even butterworth filter order: ');
BWhz = input('Enter filter bandwidth in Hz: ');
BWrad = BWhz*2*pi;
[B,A] = butter(order/2,[(ctrFreq-BWrad/2) (ctrFreq+BWrad/2)], 's');
sysF = tf(B,A);

%% get filter phase
[Mf,PHf] = bode(sysF,ctrFreq);
thetaC = PHcd + PHf;
```

```
%% Find required phase correction
thetaA = 180 - thetaC;

%% make sure angle is 0 < thetaA < 360
if thetaA > 360 | thetaA < -360
    thetaA = thetaA - floor(thetaA/360)*360;
end

%% convert angle to radians for all-pass filter pole calculation
taRad = thetaA*pi/180;

if thetaA > 0 & thetaA < 180
    filtPole = ctrFreq/cot(taRad/2);
    G = 1;
    num = [1 -filtPole];
    den = [1 filtPole];
    sysF2 = tf(num,den);
elseif thetaA > 180 & thetaA < 360
    taRad = taRad - 2*pi;
    filtPole = -ctrFreq/tan(taRad/2);
    G = 1;
    num = [1 -filtPole];
    den = [1 filtPole];
    sysF2 = tf(-num,den);
elseif thetaA == 180
    disp('No all pass required');
    filtPole = 0;
    G = 1;
    sysF2 = 1;
else
```

```
    disp('No all pass required, inverting gain value needed');
    filtPole = 0;
    G = -1;
    sysF2 = 1;
end

Q1 = [2 1;3 6;5 2];
sysCLb = connect(append(series(series(sysF,sysF2),G),sysC,sysD),Q1,1,5);
sysCLc = connect(append(1,sysC,sysD),Q1,1,5);

figure(1)
pzmap(sysCLc);
title('Pole Zero Map of Open-loop System');

figure(2);
rlocus(-sysCLb);
title('Root Locus of Control Path');
axis([-400 200 -2500 2500]);

%% get filter gain
absG = input('Enter absolute filter from Root Locus plot: ');
filtG = G*absG;

%% Display filter transfer functions.
disp(' ');
disp('Control Filter TF function: ')
sysF

if filtPole
    disp('All-pass filter TF function: ');
```

```
    sysF2
end

%% Generate OL/CL frequency response plots.
sysTemp = append(sysD,sysN,sysC,series(series(sysF,sysF2),filtG),1);
Q = [1 5;2 6;4 1;5 7;6 4;7 8;8 3];
sys = connect(sysTemp,Q,3,2);

if ~isempty(find(real(pole(sys))>0))
    disp('System unstable: choose a lower gain value');
else
    disp('System Stable');

    freqT = linspace(10,2*pi*300,1000);
    f = freqT/2/pi;

    [MTmp,PHTmp] = bode(sysOL,freqT);
    Mol = 20*log10(abs(squeeze(mp2h(MTmp,PHTmp))));
    PHol = angle(squeeze(mp2h(MTmp,PHTmp)))*180/pi;

    [MTmp,PHTmp] = bode(sys,freqT);
    M = 20*log10(abs(squeeze(mp2h(MTmp,PHTmp))));
    PH = angle(squeeze(mp2h(MTmp,PHTmp)))*180/pi;

    figure(3);
    plot(f,Mol,f,M);
    xlabel('Frequency (Hz)'),ylabel('Magnitude (dB)');
    axis([20 300 -45 10]);
    title('Bode diagram');
    legend('forward-path','closed-loop');
```

```
    T = 0:6.1e-05:.5;
    U = cos(Wns(1)*T);

    figure(4);
    lsim(sys,sysOL,U,T);
    legend('cl','ol','input');
end
```

BIBLIOGRAPHY

[1] David A. Bies and Colin Hansen. *Engineering Noise Control: Theory and Practice*. Taylor and Francis Group, New York, NY, 2003.

[2] Lord J.W.S. Rayleigh. *The Theory of Sound*. Dover Publicaions, Inc., New York, NY, 1945.

[3] U. Ingard. On the theory and design of acoustic resonators. *JASA*, **25**(6):1037–1061, 1953.

[4] Theodore-M Kostek. Combining adaptive-passive and fully active noise control in ducts. In *ASME IMECE 1997*, volume **24**, pages 293–8, Fairfield, NJ, 1997.

[5] K. Nagaya, Y. Hano, and A. Suda. Silencer consisting of two-stage helmholtz resonator with auto-tuning control. *JASA*, **110**(1):289–95, 2001.

[6] Jonathan D. Kemp and Robert L. Clark. Noise reduction in a launch vehicle fairing using actively tuned loudspeakers. *JASA*, **113**(4):1986–94, 2003.

[7] L. E. Kinsler,A. R. Frey,A. B. Coppens, and J. V. Sanders, *Fundamentals of Acoustics*. John Wiley and Sons, Inc.,New York, NY, 1982.

[8] P. A. Nelson and S. J. Elliott. *Active Control of Sound*. Academic Press, New York, NY, 1992.

[9] H. Boonen and P. Sas. Stability Improvement for Feedback Noise Control in Ducts Using A Time Delay Compensator. *International Conference On Noise and Vibration Engineering*, volume **25**, pages 9–14, Katholieke Universiteit Leuven, Belgium, 2000.

[10] S. C. Douglas. Adaptive Filters Employing Partial Updates. *IEEE Transactions on Analog and Digital Signal Processing*, **44**(3): 209–216, 1997.

[11] O. Kipersztok and R. Hammond. The Use Of Fuzzy Logic In Active Noise Control. In *3rd International Symposium on Uncertainty Modelling and Analysis*, College Park, MD, March 17-20 1995.

[12] H. F. Olson and E. G. May. Electronic sound absorber. *JASA*, **25**(1):1130–6, 1953.

[13] Jeffrey S. Vipperman, Deyu Li, Ilya Avdeev, and Steven Lane. Investigation of the sound transmission into an advanced grid-stiffened structure. *JVA*, **125**(3):257–266, 2003.

[14] Deyu Li and Jeffrey S. Vipperman. Noise transmission control studies on a chamber core composite cylinder. In *ASME IMECE 2002*, number IMECE-33069, New Orleans, LA, November 17-22 2002.

[15] Steven A. Lane and Robert L. Clark. Dissipative feedback control of a reverberant enclosure using a constant volume velocity source. *JVA*, **120**(3):987–993, 1998.

[16] C. B. Birdsong and C. J. Radcliffe. A compensated acoustic actuator for systems with strong dynamics pressure coupling. *JVA*, **121**(1):89–94, 1999.

[17] J. L. Fanson and T. K. Caughey. Positive position feedback control for large space structures. *AIAA Journal*, **28**(4):717–724, April 1990.

[18] James L. Fanson. An Experimental Investigation of Vibration Suppression in Large Space Structures Using Positive Position Feedback. PhD thesis, California Institute of Technology, Pasadena, CA, 1986.

[19] Steven Griffin and Collin Hansen and Ben Cazzolato. Feedback Control of Structurally Radiated Sound Into Enclosed Spaces Using Structural Sensing. *JASA*, **106**(5):2621–2628, 1999.

[20] Steven Griffin and Keith K. Denoyer and Alok Das. Passive Vibroacoustic Isolation for Payload Containers. *JIMSS*, **10**(5):83–87, 1999.

[21] Jesse B. Bisnette, Jeffrey S. Vipperman, and Daniel D. Budny. Active noise control using damped resonant filters. Abstract only. *JASA*, **113**(4):2228, 2003.

[22] F. Fahy. *Sound and Structural Vibration.* Academic Press, Inc., New York, 1985.

[23] M. E. Van Valkenburg. *Analog Filter Design.* Oxford University Press, New York, 1982.

[24] Texas Instruments, Inc. *Application Bulletin: Filter Design Program for the UAF42 Universal Active Filter*, 2000.

[25] Mark A. McEver. Optimal Vibration Suppression Using On-line Pole/Zero Identification. MS thesis, Virginia Polytechnic Institute and State University, Blacksburg, VA, 1999.

[26] Kevin. Farinholt. Modal and Impedance Modeling of a Conical Bore for Control Application. MS thesis, Virginia Polytechnic Institute and State University, Blacksburg, VA, 2001.

[27] Jesse B. Bisnette, Jeffrey S. Vipperman, and Daniel D. Budny. Active Noise Control Using Phase-compensated, Damped Resonant Filters. In *ASME IMECE 2002*, number IMECE2003-41831, Washington, D.C., November 15-21 2003.